Advancements of 2D speckle tracking of arterial wall movements

Albinsson, John

2017

Document Version:
Publisher's PDF, also known as Version of record

Advancements of 2D speckle tracking of arterial wall movements

John Albinsson

LUND
UNIVERSITY

DOCTORAL DISSERTATION
by due permission of the Faculty Engineering, Lund University, Sweden.
To be defended in Segerfalksalen, BMC, Lund, on May 12 at 09:15.

Faculty opponent
Professor Hevré Liebgott
CREATIS, University of Lyon

Cover illustration

Figure shows the principals of motion estimation using the block-matching method presented in Paper I. The three ultrasound images depict a skeletal muscle (extensor digitorum communis) of a volunteer. The nine crosses in each image indicates the position of the center of one kernel.

ISBN: 978-91-7753-220-0 (printed version)
ISBN: 978-91-7753-221-7 (electronic version)
Report nr: 2/17
ISRN: LUTEDX/TEEM—1108—SE
Printed in April 2017 by Tryckeriet i E-huset, Lund, Sweden

Organization: Lund University Department of Biomedical Engineering P.O. Box 118, SE-221 00 Lund, Sweden	**Document name:** Doctoral Dissertation **Date of issue:** May 12, 2017 **Sponsoring organization:** Swedish Foundation for International Cooperation in Research and Higher Education, the Knut and Alice Wallenberg Foundation, the Medical Faculty - Lund University, the Skåne County Council's Research and Development Foundation, and the Swedish Research Council
Author: John Albinsson	

Title: Advancements of 2D speckle tracking on arterial wall movements

Abstract:

Cardiovascular diseases are the leading cause of death worldwide. In order to improve the diagnostics and facilitate early interventions of cardiovascular diseases, knowledge about the physiology of the vascular system in both healthy subjects and in subjects with vascular disease is needed. In order to learn more about the physiology of the vascular system and possibly predict cardiovascular diseases, accurate motion estimations of the arterial wall is needed. It has been the aim of this thesis to develop more robust motion estimation methods for use on cine loops to investigate the entire thickness of the arterial wall.

In this thesis, the concept of 2D speckle block matching was expanded with the use of an extra kernel for improved robustness and tracking accuracy. It was shown that the use of an extra kernel reduced the motion estimation errors when using a constant kernel size (*in silico* and on phantoms), or reduced the needed size of the kernel while maintaining the level of motion estimation errors (*in vivo*). Further, a sub-sample estimation method has been developed which combines two previously presented methods: parabolic and grid slope sub-sample interpolation. It was found that by combining the two methods with a threshold determining which method to use, the proposed method reduced the absolute sub-sample estimation errors in simulated and phantom cine loops. A limited *in vivo* evaluation of estimations of the longitudinal movement of the common carotid artery using parabolic and grid slope sub-sample interpolation and the proposed method were conducted showing that the method worked well *in vivo*.

The two methods were combined to estimate the longitudinal wall movement of the right common carotid artery on 135 healthy volunteers for improved understanding of the wall movements. The results show that the pronounced variation in patterns of longitudinal movement of the common carotid artery previously shown in young healthy subjects is also present in middle-aged and older healthy subjects. However, the patterns of movement seen in middle-aged and older subjects are different from those commonly seen in young subjects, including the appearance of two additional distinct phases of movement, and thus new complex patterns of movement.

The use of ultrasound sampled at a high frame rate has the potential to visualize previously unknown information of the longitudinal movement. An iterative scheme for Lagrangian motion estimations in cine loops collected at high frame rates was developed. A phantom evaluation using ultrasound cine loops showed a reduction by an average 54% in the estimated velocity errors compared to a standard method. It also showed a reduction by an average 73 % in the estimated displacement errors. A feasibility test of tracking *in vivo* indicated good agreement with motion estimations using a low frame rate cine loop.

This thesis thus present and evaluate refined methods to measure vascular function through the estimation of longitudinal movement.

Keywords: Ultrasound, block-matching, tissue motion, longitudinal movement

Classification system and/or index terms:

Supplementary bibliographical information: ISRN: LUTEDX/TEEM—1108—SE Report-nr: 2/17	**Language:** English
ISSN and key title:	**ISBN:** 978-91-7753-220-0 (Print) 978-91-7753-221-7 (Electronic)

Recipient´s notes:	**Number of pages:** 144	**Price: No**
	Security classification:	

Signature: John Albinsson **Date: 2017-04-10**

Public defence
May 12th 2017, 09.15, Segerfalkssalen

Advisors
Associate Professor Magnus Cinthio
Department of Biomedical Engineering, Lund University

Associate Professor Tomas Jansson
Clinical Sciences Lund, Biomedical Engineering, Lund University, Lund, Sweden
Medical Services, Skåne University Hospital, Lund, Sweden

Associate Professor Åsa Rydén Ahlgren
Department of Medical Imaging and Physiology, Skåne University Hospital, Malmö, Sweden
Department of Translational Medicine, Lund University, Malmö, Sweden

Faculty Opponent
Professor Hevré Liebgott
CREATIS, University of Lyon

Board of Examination
Professor Johan Carlson
Department of Computer Science, Electrical and Space Engineering at Luleå University of Technology, Luleå

Professor emeritus Tomas Gustavsson
Department of Signals and Systems, Chalmers, Göteborg

Associate Professor Kerstin Jensen-Urstad
Karolinska Institutet, Solna

Deputy member:
Associate Professor Sven Månsson
Medical Radiation Physics, Malmö, Lund University

Chairman
Associate Professor Johan Nilsson
Department of Biomedical Engineering, Lund University

Dedication

To my loved ones

Present and absent

You can't change the world

But you can change the facts

And when you change the facts

You change points of view

If you change points of view

You may change a vote

And when you change a vote

You may change the world

—Depeche Mode

Abstract

Cardiovascular diseases are the leading cause of death worldwide. In order to improve prevention and treatment of cardiovascular diseases, knowledge about the physiology of the vascular system in both healthy subjects and in subjects with vascular disease is needed. The study of the movement of the arterial wall can increase that knowledge. Studies of the radial component of the movement of the arterial wall have already done that for centuries. However, our knowledge of the longitudinal component is scarce. Although the knowledge concerning the longitudinal movement of the wall of the common carotid artery has increased significantly since it was first reported a decade ago, the function of and the mechanisms underlying this movement are still not fully understood, and further research is needed. Our experience is that only images of the highest quality are likely to give accurate and reliable longitudinal motion estimations of the arterial wall using block-matching. As capturing that level of quality is demanding also for very skilled sonographers, the numbers of collected cine loops, i.e. sequences of ultrasound images, to be useful for longitudinal motion estimations can be somewhat limited. It is thus of interest to develop more robust motion estimation methods for use on cine loops of lower image quality to investigate the entire thickness of the arterial wall. In order to not limit the use of our methods, the aim while developing the presented methods were a generic *in vivo* use on all tissue with a reasonable stable speckle pattern.

In this thesis, the concept of 2D speckle block matching was expanded with the use of an extra kernel for improved robustness and tracking accuracy. Tests were performed both on how the motion estimation errors change using a constant kernel size, and conversely, what kernel size is required to maintain a constant motion estimation error. It was shown that the use of an extra kernel reduced the motion estimation errors (mean = 48 % [in silico]; mean = 43 % [phantom]) with a constant kernel size, or reduced the size of the kernel (mean = 19 % [*in vivo*]) while maintaining the level of motion estimation errors.

Further, a sub-sample estimation method has been developed which combines two previously presented interpolation methods: parabolic and grid slope. It was found that by combining the two methods with a threshold determining which method to use, the proposed method reduced the absolute sub-sample estimation errors *in silico* and phantom cine loops compared to sub-sample interpolation of the image (14 %), parabolic sub-sample interpolation (8 %), and grid slope sub-sample interpolation (24 %). A limited *in vivo* evaluation of estimations of the longitudinal movement of the common carotid artery using parabolic and grid slope sub-sample interpolation and the proposed method were conducted. The magnitudes of the movement in two cine loops from the same volunteer were used to calculate the coefficients of variation of the three sub-sample methods which

were found to be 6.9, 7.5, and 6.8 %, respectively. Moreover, the proposed method is computationally efficient and has low bias and variance.

The two methods were combined to estimate the longitudinal wall movement of the right common carotid artery on 135 healthy volunteers for improved understanding of the wall movements. The results show that the pronounced variation in patterns of longitudinal movement of the common carotid artery previously shown in young healthy subjects is also present in middle-aged and older healthy subjects. However, the patterns of movement seen in middle-aged and older subjects are different from those commonly seen in young subjects, including the appearance of two additional distinct phases of movement, and thus new complex patterns of movement. Three of the five phases showed a significantly correlation with age. Also, indications of changes in the prevalence of different patterns of the longitudinal wall movement with age were seen.

The use of ultrasound sampled at a high frame rate has the potential to visualize previously unknown movement patterns. However, the displacement of the studied object will mostly be very small between two consecutive images which will result in large relative estimation errors if using block-matching. Thus, an iterative scheme for Lagrangian motion estimations in cine loops collected at high frame rates was developed. A phantom evaluation using ultrasound cine loops sampled at 1300 frames per second showed a reduction by an average 54 % in the estimated velocity errors (set velocities 1.1 and 2.2 mm/s). It also showed a reduction by an average 73 % in the estimated displacement errors (set displacements 0.6 and 1.1 mm). A feasibility test of tracking *in vivo* indicated that the estimations agreed well with estimations using a low frame rate.

In conclusion, in this thesis three methods are presented for robust and fast motion estimation using 2D speckle block matching. The methods have been tested using cine loops collected *in silico*, on phantoms, and (most importantly) *in vivo,* and they have shown robust tracking performance. The methods could be important tools for estimating motions *in vivo* and thus for furthering our knowledge about the physiology, e.g. of the vascular system, in both healthy and diseased individuals.

Populärvetenskaplig sammanfattning

Hjärt- och kärlsjukdomar är den vanligaste dödsorsaken i världen och för förbättrad diagnostik och tidiga insatser är kunskap om fysiologin i det mänskliga kärlsystemet hos både friska och sjuka personer nödvändig. Därför har den radiella rörelsen, diameterförändringen, hos kärlväggar undersökts sedan länge. Diameterförändringen är det som känns när man tar pulsen. Ett mer outforskat område är den relativt nyupptäckta längsgående rörelsen i våra kärlväggar. Det har spekulerats att denna rörelse kan användas för att tidigt identifiera individer med hög risk att utveckla kärlsjukdom. De metoder som finns tillgängliga idag kräver bilder av allra högsta kvalitet för att göra tillförlitliga mätningar av de längsgående rörelserna i hela kärlväggens tjocklek. Det är således av intresse att utveckla mer robusta metoder för mätningar av rörelser i sekvenser av ultraljudsbilder för att dels förbättra vår kunskap av den längsgående rörelsen i våra kärlväggar men även för att kunna använda ultraljudsbilder av normal bildkvalitet.

I denna avhandling presenteras tre snabba och robusta metoder för mätning av rörelser i sekvenser av ultraljudsbilder. Metoderna har vid tester på rörelser i simulerade ultraljudsbilder, ultraljudsbilder av objekt som efterliknar mänsklig vävnad, och (slutmålet) ultraljudsbilder från människor, producerat mätningar vars noggrannhet är signifikant bättre (i flera fall 50 %) än jämförbara metoder.

Ett sätt att mäta rörelser är genom att jämföra en urklippt kvadrat av en bild (en mall) med flera kvadrater i en efterföljande bild, s.k. blockmatchning. Kvadraten i den nya bilden med störst likhet med mallen anses vara samma område. En rörelse beräknas sedan som skillnad i position för mallen och den utpekade kvadraten. En metod för blockmatchning innehåller normalt tre steg: det första steget säger hur metoden ska leta efter området med den största likheten. Det andra steget mäter likheten mellan mallen och ett område i bilden med hjälp av en matematisk formel. Det första och andra steget bestämmer tillsammans en rörelse till ett heltal. Då de flesta rörelser är av en längd mellan två heltal skulle ett heltalssvar ge onödigt stora fel. Därför används det tredje steget för att bestämma rörelsen till ett decimaltal baserat på resultatet från första och andra steget, s.k. sub-pixel bestämning.

Denna avhandling består av fem vetenskapliga studier. I dessa studier har vi undersökt de tre stegen som används vid blockmatchning och utvecklat metoder för en förbättrad bestämning av rörelser. Vi har infört användandet av två mallar i stället för en och dessutom använder vi en sökmetod som minskar beräkningstiden jämfört med

konventionella metoder. Efter en undersökning av hur andra steget påverkar det tredje steget, kunde vi utveckla en ny metod för sub-pixel bestämning. En möjlighet att skaffa mer kunskap om rörelser är att använda ultraljudsbilder som har samlats in med en hög bildhastighet. Problemet för en blockmatchningsmetod är då att rörelserna per bild blir väldigt små, vilket leder till att den ofrånkomliga mätosäkerheten i rörelsebestämningen ger stora sammanslagna fel. Genom upprepade rörelsebestämningar mellan bilder på olika tidsavstånd har vi kunnat förbättra noggrannheten i bestämningen av både den lokala och totala rörelsen. Vi har även i ultraljudsbilder insamlade vid normal bildhastighet (ca 50 bilder per sekund) uppskattat den längsgående rörelsen i halspulsådern på mer än 100 friska frivilliga forskningspersoner. Fem distinkta faser i rörelsen kunde definieras (varav två hittills okända) och individerna kunde delas in i fem olika grupper. Alla grupper innehöll inte alla faser och de hade olika förhållanden mellan storleken på faserna i sina rörelsemönster. Även om detta har utökat vår kunskapsbas om kärlväggens fysiologi och det normala åldrandet av kärlväggen, så behövs det mer forskning för att använda denna nya kunskap inom sjukvården.

Acknowledgements

Nine years ago, I stepped into Elmät looking for a Master thesis project. The project turned into a manuscript and after some detours it suddenly transformed into a Doctoral thesis. Now when it is time to summarize this work, there are a number of individuals that have been very important and helpful along the way to whom I would like to show my gratitude.

Thank you Magnus! Without your support and enthusiastic response to my work this goal would never have been reached. People has commented my struggle to get my papers published, but I think that your struggle to battle my opinion on the results and to get me going in the right direction have been greater. Naturally, this project hadn't existed at all if not Sofia Brorsson had asked you to do it, but it was you Magnus who pushed the whole distance. Please take care.

But we were not without help. From the early manuscripts to the final version of this thesis, the proofreading of Tomas has been fundamental for the quality of the text. Åsa, you entered a little later and still claim that you do not understand the technical stuff in my manuscripts. However, your questions and skillful reviewing have several times forced me to take a step back and to re-write my texts for them to be understandable. A great thank you to both of you.

A special thanks goes to Maria and Tobias, to whom I said "Hello" in the master-thesis-room and with whom I still share a room. The comments about our crammed room have been plenty but I have never had reason for complaints. Your presence and friendship have been a great help during this time.

During my time as a PhD-student, I have had the privilege to spend some of my time abroad. With the support given both in Florence and in Sendai, the experience of my visits were amazing and I will have great memories for the rest of my life. Thank you for your support.

I would also thank all the customers of the Cookie Empire and everyone else that made all my coffee breaks, or rather cookie breaks, a pleasant pause from work. A special thanks goes to the leader of the pack, Johan, whose support has been crucial during my time as a PhD-student.

I would like to greatly acknowledge the sponsoring organizations. Without the financial support from the Swedish Foundation for International Cooperation in Research and Higher Education, the Knut and Alice Wallenberg Foundation, the Medical Faculty,

Lund University, the Skåne County Council's Research and Development Foundation, and from the Swedish Research Council this work would not have been possible. Thank you!

Last, but perhaps greatest, I would like to thank my family which has been a solid support through this time even if they do not know what I have been doing.

List of publications

I. **Improved Tracking Performance of Lagrangian Block-Matching Methodologies Using Block Expansion in the Time Domain *In Silico* Phantom and *In Vivo* Evaluations**

John Albinsson, Sofia Brorsson, Åsa Rydén Ahlgren, and Magnus Cinthio

Ultrasound in Medicine and Biology, Vol. 40, No. 10, pp. 2508-2520, 2014

Author's contribution: Method development; planning of in silico set-up and ultrasound measurements; motion estimations in all cine loops and analyze of data; main author of manuscript.

II. **Tracking Performance of Several Combinations of Common Evaluation Metrics and Sub-pixel Methods**

John Albinsson, Tomas Jansson, and Magnus Cinthio

16th Nordic-Baltic Conference on Biomedical Engineering, IFMBE Procedings 48, DOI: 10.1007/978-3-319-12967_4, 2015

Author's contribution: Planning of project; simulating cine loops; motion estimations and analyze of data; main author of manuscript.

III. **A combination of parabolic and grid slope interpolation for 2D tissue displacement estimations**

John Albinsson, Åsa Rydén Ahlgren, Tomas Jansson, and Magnus Cinthio

Medical & Biological Engineering & Computing, DOI: 10.1007/s11517-016-1593-7, 2016

Author's contribution: Method development; planning of in silico set-up, ultrasound measurements, motion estimations, and analyze of data; main author of manuscript.

IV. **Phases and resulting patterns of the longitudinal movement of the common carotid artery wall in healthy humans – influence of age and gender**

Magnus Cinthio, John Albinsson, Tobias Erlöv, Niclas Bjarnegård, Toste Länne, Åsa Rydén Ahlgren

Manuscript

Author's contribution: Developing the methods used for motion estimation; participated in the classification of the movement patterns and the planned statistics, co-author *the manuscript*

V. **Iterative 2D speckle tracking in cine loops from high frame rate ultrasound**

John Albinsson, Hideyuki Hasegawa, Hiroki Takahashi, Åsa Rydén Ahlgren, and Magnus Cinthio

Manuscript – submitted 20170307

Author's contribution: Method development; motion estimations and analyze of data; main author of manuscript.

Contents

Abbreviations

2D – two dimensional

3D – three dimensional

CC – Cross-Correlation

FS – Full Search

GS15PI – sub-sample method developed in paper II

IQ – In-phase Quadrature

NCC – Normalized Cross-Correlation

RF – Radio Frequency

SAD – Sum of Absolute Difference

SSD – Sum of Squared Difference

1. Introduction

Clinical investigations and research using ultrasound is an important clinical image modality and is very likely to continue to be. Among several benefits, the high temporal resolution in an ultrasound acquisition makes it very suitable for investigating dynamic processes *in vivo* in real time. In many cases, an important step towards the sought after information is estimating the observed motions in the ultrasound cine loops.

This thesis has investigated motion estimations in ultrasound cine loops using block-matching in general, and has applied the accumulated knowledge to estimate the longitudinal movement of the intima-media complex of the common carotid artery *in vivo* in healthy volunteers. The investigations were conducted using both frame rates used in clinical investigations, and plane wave imaging for high frame rate sampling.

1.1 Outline of the thesis

The outline of this thesis is as follows: Chapter 2 introduces ultrasound and presents the fundamentals of how it works, how the image data are presented, and how the types of image data are related. Chapter 3 presents information about motion estimation methods in consecutive images in general, and some methods specifically developed for use with ultrasound. Chapter 4 describes block-matching which is the base method used in the papers presented in this thesis. Important parts of a block-matching method are defined and some basic knowledge is presented. The sources of ultrasound images and their pros and cons are presented in Chapter 5. Chapter 6 gives a description of the longitudinal movement of the arterial wall. A short description of the papers included in the thesis is given in Chapter 7 followed in Chapter 8 by a discussion relating to both the papers with some general reflections on conducting research before a summary in Chapter 9 of the primary knowledge gained during this work. The thesis is concluded in Chapter 10 with some prospects.

2. Ultrasound

The content in this chapter can be found in a variety of textbooks, e.g. [1, 2], unless otherwise specifically referenced.

2.1 Fundamentals

Sound is oscillating pressure variations travelling through a medium. Three groups of sound has been defined based on their oscillation frequency: infrasound (below 20 Hz), acoustic sound (20 Hz – 20 kHz), and ultrasound (above 20 kHz). In clinically used ultrasound, the commonly used frequencies range from 1 to 20 MHz which is a compromise between spatial resolution and the depth that is visible in the images.

The so called "pulse-echo method", i.e. a short pulse of ultrasound is transmitted into a patient and the resulting echoes received, is used to form an image of the interior of the patient (Figure 1). The echoes are a natural result of ultrasound

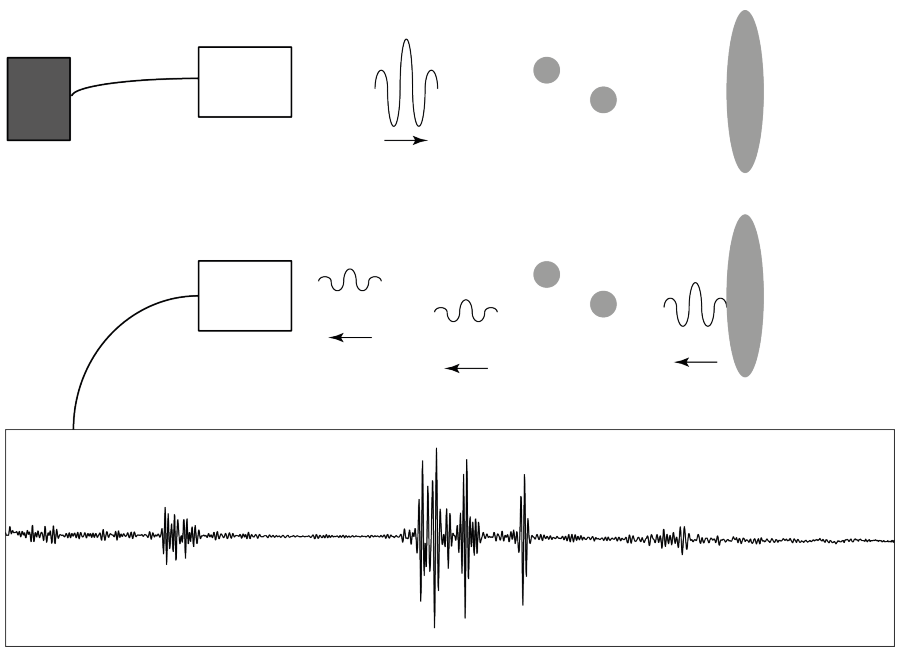

Figure 1. Stylistic representation of the pulse-echo method. On short ultrasound pulse is transmitted from the probe and reflected to varying degrees from encountered volumes with acoustic impedance differing from the surrounding tissue. A possible sampled signal (an A-line) is show at the bottom.

passing from an area with one level of acoustic impedance into an area with a different level of acoustic impedance.

$$Z = \rho * v \tag{1}$$

Here Z is the acoustic impedance, ρ is the density of the media, and v is the speed of sound in the media. The fraction of sound that is reflected is given by the reflection coefficient:

$$R_A = \frac{Z_2 - Z_1}{Z_2 + Z_1} \tag{2}$$

Here R_A is the coefficient of reflection for amplitude, Z_1 is the acoustic impedance in the current media, and Z_2 is the acoustic impedance in the next media. The difference in acoustic impedance of different types of soft tissue in the human body is usually rather low. The benefit is that while some of the ultrasound energy will be reflected when the ultrasound encounter a new acoustic impedance (typically a new type of tissue) and provide data for the image formation, most of the energy will continue deeper inside the body to potentially be reflected there. Normally, an ultrasound image is built one line (or column) at a time by transmitting a pulsed beam of ultrasound which is focused at a certain user defined depth in the patient. The beam will have a certain elevational thickness and its minimal width at the point of focus. The beam is produced by a number of piezoelectric elements in a probe. As the acoustic impedance both varies within each type of tissue and the reflecting surfaces are often not smooth, the reflected ultrasound reaching the probe will be a superimposed wave of reflections. Adding the sampled ultrasound data by timing the data from the various probe elements so the direct echoes will have been reflected at the same depth along the line to be produced will have the effect that the reflections from this point will get a constructive interference while reflections from other points will interfere destructively. This process is called beamforming. If the reflections were produced by a large structure in the body, several neighboring pixels will contain similar information and together they will form a visible structure. In many cases the reflections will be from objects that are small, unevenly shaped and/or have a small difference in the acoustic impedance towards the surrounding tissue. The reflections will be weak and depending on the angle of the ultrasound and the resulting ultrasound image will have a pattern that resembles noise. This pattern, so called speckle, is quite different from noise as it is stable over time and reproducible by repositioning the probe and the reflecting tissue in the same geometrical position. However, as the speckle pattern is created by superimposing several weak reflections, the pattern will change as the probe is

moved compared to the reflecting tissue. This is a fairly slow process often requiring a movement within the image plane in excess of 10 mm before being clearly visible.

Typically, ultrasound data are collected one line per transmitted ultrasound pulse with consecutive lines translated sideways to build a two-dimensional (2D) image. The process is then repeated to sample image data over time to study how movement of objects. Equipped with a special transducer, some modern ultrasound scanners can sample data in three spatial dimensions (3D). The data are then sampled as a stack of 2D data, where each set of 2D data is collected in an image plane parallel to the first but with a perpendicular offset. One drawback of creating an image line by line is the time needed for the collection of data which can lead to motion artifacts within an image. This is an increasing problem when sampling 3D cine loops. One solution is plane wave imaging in which an unfocused plane wave is transmitted using all elements in a transducer and all elements are used in receive (see Chapter 2.3).

Ultrasound has a number of benefits compared to other imaging modalities:

- Safety; there are no known long term risks of using ultrasound *in vivo*.
- Portability; an ultrasound machine is highly portable and is easy to move to the bed of a patient.
- Price; an ultrasound machine has the lowest price tag of the image modalities except for superficial optical systems.
- Timing; an ultrasound investigation is conducted in real time with a temporal resolution high enough to study most of the physiological events in the body. The use of plane wave imaging can further improve this resolution.
- Resolution; the spatial resolution of a state-of-the-art ultrasound machine is better than PET and SPECT, and is on par with MRI and x-ray/CT.

This makes ultrasound superior in many and diverse imaging situations. However, there are also limitations. Among the considerations of the use of ultrasound are:

- Risks; Two short term risks are heating of and implosions in the tissue, but these risks are well known and can easily be avoided.
- Gases; when used *in vivo* ultrasound cannot penetrate gas filled cavities due to the very low acoustic impedance of most gasses which excludes investigations of healthy lungs and can cause problem when investigating the intestines.
- Bones; ultrasound cannot normally enter bones *in vivo* due to the very high acoustic impedance of bones.

- Scatter and absorption; soft tissue is made up of a rather inhomogeneous material when looking on a cellular level. This causes quite an amount of signal loss as the sound waves are reflected away from the transducer. This loss is an increasing problem in severely obese patients. As both the axial resolution and loss of signal increases with the frequency of the ultrasound the operator has to optimize the used frequency.

Ultrasound is commonly used *in vivo* to investigate blood flow and soft tissue, e.g. [3-11]. The use is very diverse and has several application areas. The blood flow investigations range from functionality tests of the heart valves by estimations of the blood flows in the heart, through the blood flow in arteries, to the perfusion in the kidneys. Soft tissue investigations range from inspection of the heart muscle and the eyes to prenatal ultrasound investigations.

2.2 Ultrasound data for motion estimation

The most basic ultrasound signal is the amplified voltage measured from a piezoelectric probe. Displaying the received echoes after a transmitted ultrasound pulse on an oscilloscope gives what is called an A-mode line. By repeatedly transmitting and sampling the A-mode line at a reasonable pace without displacement of the transducer, an M-mode image is produced by displaying the A-mode lines side-by-side (Figure 2). The M-mode image facilitates the possibility to see how the studied reflectors move by a comparison of the lines. If the A-mode lines are sampled at slightly different horizontal positions or with slightly different angle towards the surface, the combined lines will form an image over the spatial distribution of the reflectors. It is also possible to create 3D images by further shifting the probe perpendicular to the previous scan plane. However, even if an image can be acquired by translating a single probe, the spatial resolution will be poor and today the ultrasound probe contains an array of piezoelectric elements to improve image quality.

The ultrasound data sampled from a number of piezoelectric elements are beamformed into a line of data similar to an A-mode line but with an improved image quality and is mostly called RF (radiofrequency) data when an image is to be sampled. The beamformed data (RF data) is converted by filtering, IQ-demodulation, and resampling into In-phase Quadrature (IQ) data [12]. This converts the sampled real valued pressure data into a complex number with an amplitude and a phase starting at zero for the first sampled RF data. The number of data points are also normally reduced and, if performed correctly, the RF data can be reformed from the IQ data. The magnitude of the IQ data have much larger

dynamic range than any screen, and thus the logarithm with base 10 of the data are calculated before presenting it on a screen as a brightness (B-) mode image with the value of the data shown as different levels of pixel intensity (Figure 2).

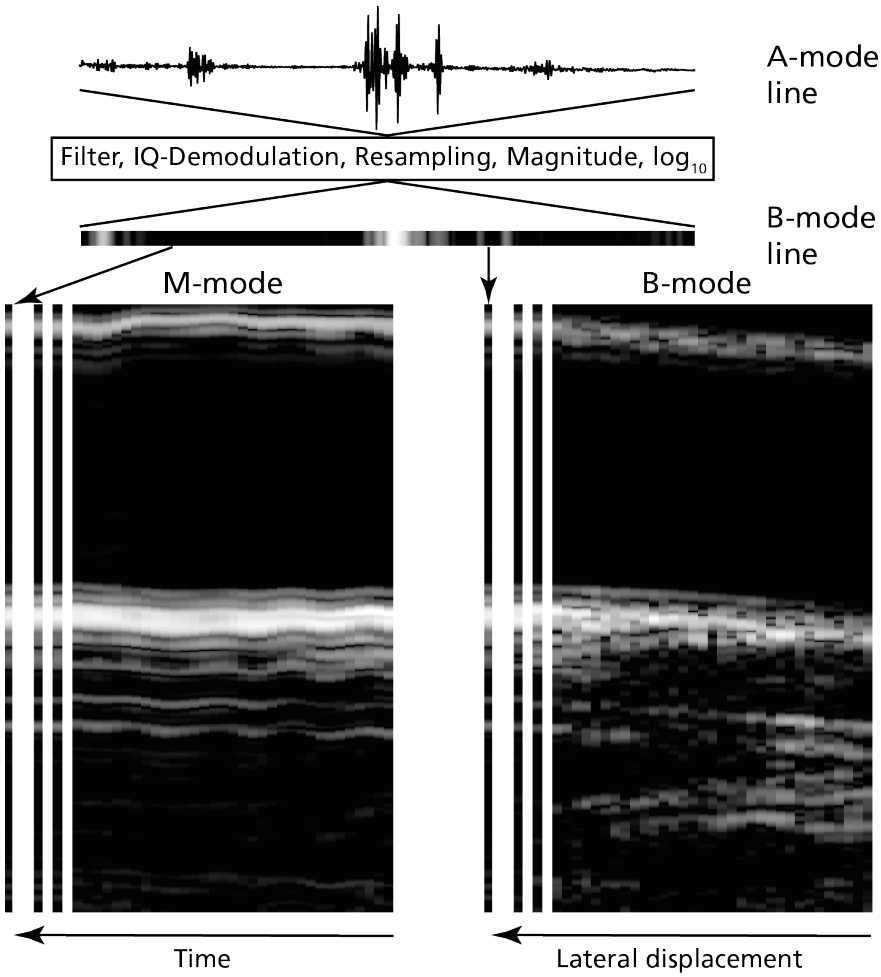

Figure 2. From A-mode line through B-mode line to M-mode image or B-mode image. From each A-mode line or line of RF (radiofrequency) data, one B-mode-line is created. Sampling several lines can create one of two images depending on the position of the probe at each sampling; if the same position were used the sampled lines results in a M-mode image while a translation of the probe results in a B-mode image.

Many types of motion estimation using ultrasound data involves the 2D (or lately 3D) data. Earlier it was most common to use RF data as the calculated motion estimations were more accurate. Today the benefit of using RF data is still the higher axial data density. The main drawback is the limited access of the RF data especially

when using clinical ultrasound machines. A lesser limitation is the large amount of data involved using RF data. The benefits of IQ data are the possibility to convert the data into both RF data and B-mode data, the access to the phase data, and usually a smaller amount of data compared to RF data. Again, the main drawback is the limited access of the IQ data especially when using clinical ultrasound scanners. The main benefits of using B-mode data are the ease of accessing the data. The DICOM data available on most ultrasound scanners, i.e. the B-mode data presented in an international standard, are of the highest quality. A drawback is the reduced axial resolution. A comparison of motion estimation accuracy using B-mode and RF data were made in Paper III and further discussed in chapter 7.3.

2.3 Plane Wave Imaging

The concept of ultrafast ultrasound imaging, i.e. more than 1000 frames per second, was introduced in 1977 by Bruneel *et al* [13] but the technology at the time was not mature for an implementation. It would demand hundreds of parallel data handling systems of a more modern fabrication before a realization using pulsed ultrasound would be presented in 1999 [14]. In order to reach this high frame rate, the number of ultrasound transmissions had to be reduced. This is achieved by using one broad plane, or unfocused, ultrasound wave to insonify the entire volume of interest. Several or all available transducer elements are then used to sample the ultrasound echoes from the volume.

Early implementation of plane wave imaging had problems with a reduction of contrast levels and to some extent spatial resolution [15]. In order to increase the image quality in various applications, compounding based on incoherent averaging [16] and coherent summation has been proposed [17]. Another important part of the improvement of plane wave imaging was the concept of synthetic aperture imaging [18, 19].

The major benefit of plane wave imaging is its very high temporal resolution and has thus made it possible to further study transient phenomena *in vivo*, e.g. shear wave elastography [20], pulse wave velocity [21, 22], Doppler imaging [23], vector flow imaging [24], and functional ultrasound [25].

3. Motion estimation

Motion estimation can be conducted in a number of ways. This chapter starts with a description of the two viewpoints of motion, i.e. Eularian and Lagrangian. It continues with an overview of motion estimation using sequences of images in video, excluding a large group of methods using block-matching (which is treated in Chapter 4). This chapter ends with a description of methods for estimating motion using ultrasound.

3.1 Eularian vs Lagrangian

The concepts of Eularian and Lagrangian viewpoint on movement [26] is mostly used in fluid mechanics and within research areas using movement of particles. With a Eularian viewpoint (Figure 3) the starting position is the same in each frame and thus a **different** particle or parcel of particles is tracked in each frame. With a Lagrangian viewpoint the **same** particle or parcel of particles is tracked from one image to the next throughout a sequence of images. Transforming motion estimations obtained with a Eularian viewpoint into a Lagrangian viewpoint, or vice versa, is possible. However, the accuracy of the transformation is highly dependent on the density of the motion estimations, the complexity of the investigated field of motion, and the accuracy of the motion estimations.

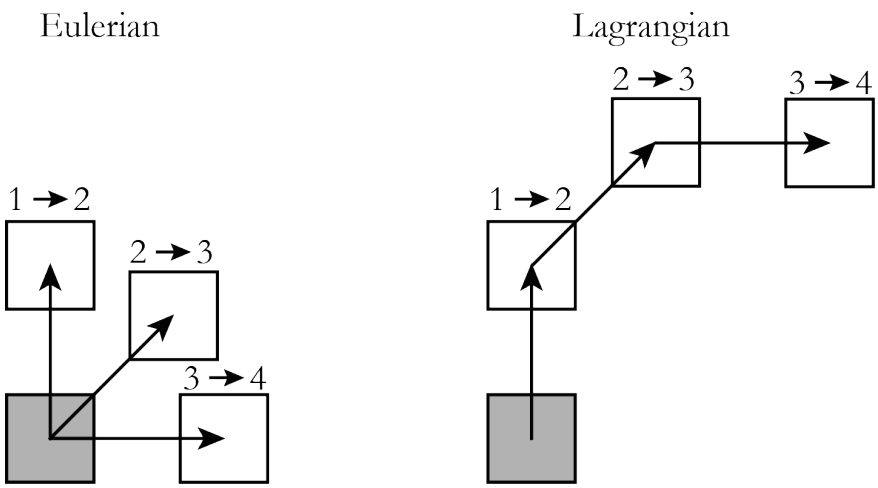

Figure 3. Eularian and Lagrangian viewpoints on motion estimations. The gray square in each viewpoint shows the same kernel. The entire images are moved with the same velocity and thus the arrows are identical in both viewpoints.

The optimal viewpoint of a motion depends on the desired density of the motion estimations. The benefit of a Eularian viewpoint is the lack of accumulated errors as each motion estimation starts anew in each image. It is also possible to discard motion estimations which are obviously erroneous if holes in the field of estimations are acceptable and/or making a better estimation using spatial filters. However, if the number of motion estimations are low and/or the motion estimations have a large variance, the use of a Lagrangian view could be beneficial. The Lagrangian viewpoint demands that the position of the object/s of interest can be accurately estimated throughout the sequence of images. If the number of objects of interest is low this will highly reduce the number of calculations needed for a complete motion estimation. However, the accuracy of the motion estimations is highly dependent on the accumulated tracking error for each object.

One benefit with a Lagrangian viewpoint is that plotting the estimated position in the cine loop is an easy way to judge the correctness of the motion estimations by visual inspection. This can be performed whether the true movement is known or not. If the position of a kernel remains close to the chosen structure or speckle, the user can be assured that the motion estimation correctly tracks the motion. This possibility is severely limited when using a Eularian viewpoint.

Overall: A Lagrangian viewpoint is recommended when a sparse density of motion estimations is needed, and a Eularian view is recommended when a dense density of motion estimations is needed.

3.2 Motion estimation in video images

Motion estimation in TV/video is frequently used in compression of the image signals. The most commonly used group of methods is block-matching (see Chapter 4). Other methods do exist though many of them are more common outside video compression. A comparison of estimating motions in video and in ultrasound cine loops is mostly relevant when using ultrasound B-mode data as IQ and RF data incorporates more usable data, i.e. phase data. There exist two major differences between video and B-mode data: 1) video has much more clearly defined objects, e.g. houses, cars, and humans; 2) the difference in velocity in a small region of an image is likely much higher in video, e.g. two meeting cars, while ultrasound images normally have a smoother velocity field.

The presence of distinct objects give access to tools when estimating motion in video that are rather useless in B-mode data, e.g. segmentation of an image and individual tracking of the segments. Structures and textures in an image also promote the use of optical flow estimations, which constitutes a large group of methods. A dense

optical flow estimation tries to match every pixel in an image with a pixel in another image. Although several assumptions exist, the most common is that the intensity of a pixel should be constant between images [27] which is not always true. Another source of ambiguity is the need of a clear structure, preferably a point or corner, to adequately estimate the motion of a pixel. This can be solved by defining additional information, e.g. texture and structure, of the pixels surrounding the pixel of interest. If the intensities of a number of other pixels are used we come close to classifying the method as a block-matching method instead.

Phase-correlation schemes use fast Fourier transforms and works with the phase correlation matrix or normalized cross power spectrum $Q(u,v)$ for motion estimation [28].

$$Q(u,v) = \frac{B(u,v)A(u,v)^*}{|A(u,v)A(u,v)^*|} = e^{-i(ux_0+vy_0)} \tag{3}$$

where (u, v) are the Fourier domain coordinates, A and B are the discrete Fourier transforms of two matrices with image data, * indicates the complex conjugate, and (x_0, y_0) are the displacement between matrices A and B. The values of (x_0, y_0) can then be determined as a plane [29] or as lines in a plane [30]. It is also common to work with the phase correlation surface after calculating the inverse discrete Fourier transform of the phase correlation matrix. For a high accuracy of the displacements (x_0, y_0), sub-sample estimation of (u, v) is needed. Phase-correlation schemes have also shown good results in estimating large rotations, scalings, and translations [31].

3.3 Motion estimation using ultrasound

Several groups of methods exist for motion estimation in ultrasound images with Doppler being the most commonly used, but speckle tracking (see chapter 4), ultrasound reflectors, and ultrasound phase data are also used.

3.3.1 Doppler

The Doppler shift in ultrasound is a change in the frequency between the transmitted and received frequencies caused by a relative motion of a reflecting object between the transmitter and receiver.

$$f_D = \frac{2f_t v \cos\theta}{c} \tag{4}$$

Here f_D is the Doppler shift, f_t is the transmitted frequency, v is the speed of the moving object, c is the speed of sound in the medium, and θ is the angle between the direction of the relative velocity and the direction of the transmitted sound. The main drawbacks of using the Doppler shift for motion estimation is well known:

the angle dependency of the Doppler shift; also, for low velocities the shift will be very small and prone to be noisy. Estimating the Doppler shift uses two methods for transmitting: continuous and pulsed ultrasound. Continuous ultrasound has one transmitter and one receiver with the investigated volume being in the area where the ultrasound beam of the transmitter and field of view of the receiver overlaps. The estimation of the Doppler shift in this area is continuous and no spatial information is gained. The pulsed Doppler uses the same transducer for transmit and receive of the ultrasound. A time gate on the received ultrasound set by the user defines the investigated volume. For the continuous Doppler, the Doppler shift is estimated as a direct difference between the transmitted and received frequencies. The pulsed Doppler cannot do that due to absorption in the media between the transducer and the investigated volume which should cause a downshift in the center frequency. Estimation of the Doppler shift is instead estimated as a phase shift detected between successively transmitted ultrasound pulses. The direction of the detected movement is determined through use of quadrature sampling. However, the repetition frequency of the transmitted pulse has to be sufficiently high compared to the investigated velocity in order to avoid aliasing. For both continuous and pulsed Doppler the velocity estimation is normally made in one volume though special versions exist were multiple estimations are made along a line [32].

For motion estimations in an area of an ultrasound image, power or color Doppler can be used. They are both utilizing pulsed Doppler as transmission mode but the results are presented somewhat differently. Color Doppler presents both direction (from or towards transducer) and mean magnitude of motion in a small area. Power Doppler uses the energy of the Doppler shift to estimate the mean magnitude of motion in an area (no direction). However, both methods lack angle correction, the estimated values are less accurate, and each estimation usually covers larger volumes than both continuous and pulsed wave Doppler. Also, as the methods samples the Doppler shift by repeated pulses, a too low pulse repetition frequency will lead to aliasing of the estimations.

Estimation of Doppler shift is primarily used for investigations of blood flow as the estimated velocities are more trustworthy and stable compared to estimating the Doppler shift for tissue motion due to the higher velocities to estimate. However, the accuracy of the estimation of the Doppler shift decreases with increased spatial gradient of a velocity within the sampled area. Another benefit of estimating the Doppler shift is the possibility to listen to the shift by sending the signal to a loudspeaker as the Doppler shift of the blood flow in many of major vessels is in the audible range. The chosen size of the investigated volume when estimating the

Doppler shift follows the same rule as most motion estimation methods; using a large area/volume will mostly give a better motion estimation, but the estimate will be of the average movement in the investigated area/volume.

3.3.2 Other techniques using ultrasound

If the estimated motion is very small, i.e. smaller than half the wavelength of the ultrasound (about 0.1 mm @ 7.5 MHz) it is possible to estimate motion using the phase of RF or IQ data. Such small motions have been investigated in e.g. heart wall vibrations [33], artery-wall strain [8], and magneto-motive ultrasound [34].

One problem when estimating motion in plane wave images is the often minimal movement between two consecutive images due to the high frame rate. One solution is to use the phase of the complex cross-correlation between the kernel and the blocks. This has been shown axially by Pesavento *et al.* [35] and laterally by Chen *et al.* [36]. A recurring problem using ultrasound images is the problem of estimating lateral motions as the spatial resolution normally is lower in the lateral direction. By use of a two-peaked apodization, i.e. transverse oscillation [37], it is possible to introduce a controlled lateral phase pattern when beamforming the ultrasound data with an increase of the lateral motion estimation accuracy [38]. The drawback of these implementations is the need for it to be part of the beamforming of the image data which is not always possible. However, it was discovered that it indeed was possible, with only minor degradations of tracking accuracy, to introduce transverse oscillations in both beamformed RF data and in B-mode data using either convolution or filtering [39]. As when using the phase of RF data in the axial direction, the maximal length of movement to be estimated is half a wavelength of the oscillations.

4. Tracking using block-matching

Block-matching, or speckle tracking, is a commonly used method for motion estimation. There exist a number of different implementations for 1-D, 2-D, and 3-D data using Both RF and B-mode data, e.g. [4, 40-45]. But every block-matching method have some common characteristics.

4.1 Parts of a speckle tracking method

Using speckle tracking, the user selects an area within an image for which motion should be estimated with the help of another image depicting the same objects. However, it is sampled at a later time instance at which time some or all objects might have moved. The selected area in the first image (a **kernel**) has a size set by the user. A speckle tracking method searches in the second image for an area (a **block**) with the highest similarity to the kernel. In order to succeed, the speckle tracking method needs: a method for determining similarity by calculating **evaluation metric values** which gives a numerical value to the similarity between the kernel and each block with which it is compared; it needs a **search methodology** to know which blocks to compare to the kernel; and, for increased tracking accuracy, a **sub-sample estimation method** is needed. A speckle tracking method can use additions to the mentioned parts, but the kernel, evaluation metric method, and the search methodology are required.

4.2 Kernels

A kernel is an area of an image often containing an object of interest which the user wants to find in another image. For practical reasons, the kernel shape is most commonly chosen as a rectangle. In general, increasing the size of the kernel results in more accurate motion estimations. If there are velocity variations within the kernel the most prominent feature is likely to dominate the motion estimation. Increasing the velocity inhomogeneity within a kernel is likely to decrease the accuracy of the motion estimations. This can give a situation were increasing the area of the kernel will result in a decreased tracking accuracy.

Sampling of the kernel in an image is simple when using a Eularian viewpoint. The position of the kernel is a given in each image, so direct use of the sampled values in the image within the perimeter of the kernel solves the problem. However, when using a Lagrangian viewpoint the intention is to track the same particle or parcel of particles throughout a number of images. Given that most of the movements in a

series of images are decimal, the center position of the kernel will be in-between sample values in most of the images. Thus, sampling of the kernel directly from the image data is not advisable. A number of solutions exist:

a) Keep using the old kernel. If the changes of the interesting parts of the images are limited, using the old kernel makes sure that we track the interesting object but the larger the changes in the image the more likely the risk for incorrect tracking.
b) Resample the kernel using the sampled values closest to the estimated position in the image. The method is quick and easy but the risk is very high that the difference between the position of used data and the object to track will increase over a number of images and we will track something else.
c) Correction value for the position. The kernel is renewed by using the sampled values in the image closest to the estimated position in the image (as in b) AND a correction value, i.e. the distance between the estimated position and position of the used samples. The correction value is added to the estimated position in the next image and becomes the estimated position for the kernel in this image. This corrects for the difference between the position of the used kernel and the position of the tracked target. The method is quick and easy with a low risk for drift of the kernel from the original target.
d) Interpolation of image data. The most common method for resampling the kernel is to interpolate the sampled values [46] in the image and using the interpolated values closest to the estimated decimal position. The method is somewhat time consuming but very reliable.
e) Prediction of the kernel. Using the sampled values in previously used kernels, the data in the new kernel is predicted, e.g. using Kalman filters [47].

4.3 Evaluation metric values

The concept of speckle tracking is to find the block most similar to the kernel. This can be achieved by calculating an evaluation metric value between the kernel and a block in order to estimate the similarity between them. In order to find the best matching block in the next image, a search methodology is used to determine the number of comparisons to calculate. The most commonly used methods are (in alphabetic order):

Cross-Correlation (CC)

$$\alpha = \sum_{i=1}^{i=l} \sum_{j=1}^{j=k} \left(X_{i,j} - \bar{X}\right)\left(Y_{i+m,j+n} - \bar{Y}\right) \tag{5}$$

Normalized Cross-Correlation (NCC)

$$\alpha = \frac{\sum_{i=1}^{i=l} \sum_{j=1}^{j=k} (X_{i,j} - \bar{X})(Y_{i+m,j+n} - \bar{Y})}{\sqrt{\sum_{i=1}^{i=l} \sum_{j=1}^{j=k} (X_{i,j} - \bar{X})^2 \sum_{i=1}^{i=l} \sum_{j=1}^{j=k} (Y_{i+m,j+n} - \bar{Y})^2}} \tag{6}$$

Sum of Absolute Difference (SAD)

$$\alpha = \sum_{i=1}^{i=l} \sum_{j=1}^{j=k} \left|X_{i,j} - Y_{i+m,j+n}\right| \tag{7}$$

Sum of Squared Difference (SSD)

$$\alpha = \sum_{i=1}^{i=l} \sum_{j=1}^{j=k} \left(X_{i,j} - Y_{i+m,j+n}\right)^2 \tag{8}$$

Here α denotes the evaluation metric value; m and n denotes the displacement between the kernel and the block; l and k denotes the size of the blocks; $X_{(i,j)}$ and $Y_{(i,j)}$ denotes the pixel values at position (i, j) in the kernel and the compared block, respectively, while $\bar{X}$ and $\bar{Y}$ denotes the average pixel values of the kernel and the block.

A major difference between the four methods is that when using CC and NCC the user searches for the *maximum likeness* while when using SAD and SSD the user searches for the *minimum difference*.

One benefit of using NCC is its normalization which reduces the influence of the average intensity in the images. Fluctuations in the average intensity can reduce the tracking accuracy of the other methods. NCC is mostly considered to have the highest stability and give the best tracking accuracy but it uses more computational power.

4.4 Search methodologies

The basic search method to find the block most similar to the kernel is to compare the kernel to all possible blocks in the image, i.e. a full search (FS). Comparing the kernel to all blocks in an image is rather inefficient and in most cases unnecessary as the expected motion of the kernel is limited to a fraction of the size of the image. Thus using a priori information about the likely length of the motions to estimate, a region of interest is chosen in which a comparison between kernel and all possible blocks is conducted. As the region of interest must be larger than the maximal motion for a possible correct estimate, the size of the region of interest is a balance

between the time needed for calculating the evaluation metric values for all blocks and the risk of having a motion with a size larger than the region of interest.

Plotting the evaluation metric values for a FS will show a sampled surface depicting a bowl (Figure 4) or top depending on the used method for calculating the evaluation metric values. Study of the surface shows that it can in most cases be considered smooth in an area close to its extreme point. This gives the possibility to use so called sparse search methods that only calculates the evaluation metric values for a selected number of blocks. This reduction in blocks comes from clever picking of blocks in conjunction with iterative searching. The surface of the evaluation metric values is thus estimated and the block closest to an extreme point is chosen as center for the next iteration.

The sparse search methods can further be divided in two groups: one group with a finite number of iterations, e.g. three step search [48], four step search [49], and orthogonal search algorithm [50]. The finite number of iterations results in a restriction that the method cannot investigate every possible block in an image and in principle the method will have a set region of interest. The second group of sparse search methods, e.g. hexagon search [51] and Adaptive Rood Pattern Search [45],

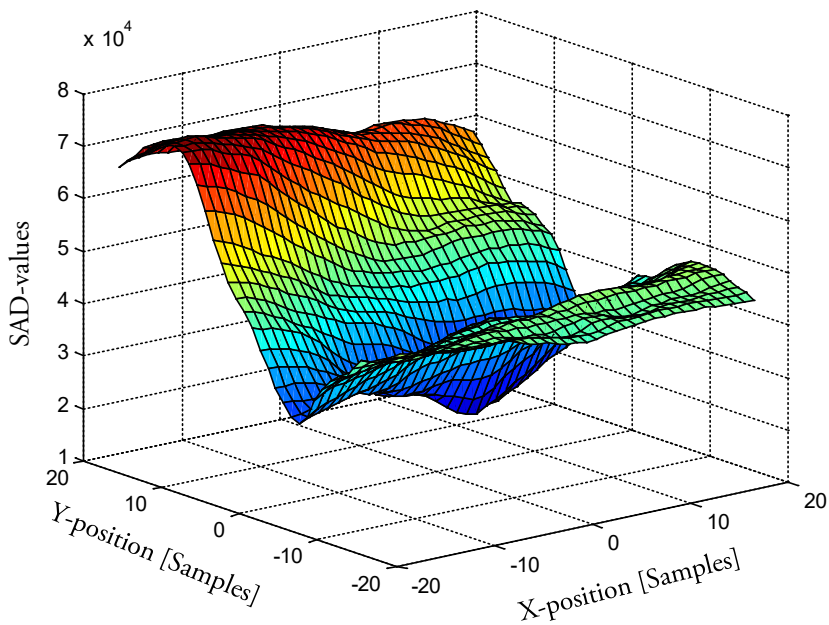

Figure 4. Similarity calculated between a kernel and all possible blocks in the next image in a region of interest using Sum of Absolute Difference (SAD).

differs in that the iterations do not stop until an extreme point has been found. The used blocks are carefully selected in a pattern determined by the method with the goal to iteratively search for the extreme point on the surface. The iterative search removes the need of a region of interest and thus removes the risk of having a motion with a size larger than the region of interest. As the methods only investigates a limited number of blocks, the number of calculations is reduced. However, as the iterations can converge on any extreme point, there is a risk that the point of convergence is a local extreme point and not the searched for global extreme point.

In most cases the kernel size is fixed during the search. A variation of the FS is to do an iterative FS starting with a large kernel size and using the estimated motion of the kernel as a criterion when reiterating the motion estimation with a smaller kernel size [52, 53]. The starting large kernel size will then give a high accuracy of the "global" motion in the image while the later smaller kernels will zoom in on the local motion. The smaller kernels will have a higher accuracy than expected by their size as they have a priori information of the motion from the large kernels used as a restricted search region.

A problem for all methods is repeated structural patterns in the image. The patterns have the possibility of creating a number of extreme points in the surface of evaluation metric values with a risk of choosing the incorrect point depending on the similarity of the values in the various extreme points. This problem is typically higher using RF data (primarily in the axial direction) than using B-mode data. The risk of finding a false extreme point is higher when using sparse tracking methods than using FS.

4.5 Sub-sample estimation methods

The sub-sample estimation methods are needed to decrease the motion estimation errors from the minimal average error of one fourth sample achieved without use of any sub-sample estimation method. This minimum estimation error assumes motions that are evenly distributed on the decimal level in space and time. Most sub-sample estimation methods can be divided into one of three groups depending on how the sub-sample estimation is performed: interpolation of the image data, interpolation of the evaluation metric values, and mathematical estimation using evaluation metric values.

a) Interpolation, or up-sampling, of the image data is a reliable method for sub-sample estimation of motion. Several methods can be used for interpolation but methods resulting in a continuous derivate over pixel borders, e.g. cubic [46] or bicubic interpolation, are recommended (see

Paper II). The improvement of the resolution depends on the interpolation factor. The drawback of this group of sub-sample estimation methods is the need for computational power. Though interpolation of the image data is fairly fast today, a new motion estimation using the interpolated image data is required with a calculation time correlated to the square of the interpolation factor. Also using a large interpolation factor (100+) will produce large amount of interpolated data which increase the computation times due to the handling of the data.

b) Interpolation, or up-sampling, of the evaluation metric values uses the fact that the surface of the evaluation metric values can be considered to be smooth close to the searched-for extreme point (Figure 4). However, the up-sampling of the evaluation metric values should not only result in a higher density of values but also be able to give both a new position and a new magnitude for the extreme point if a sub-sample position is correct. One solution is to use a filter [54] for the interpolation. The result of the method improves with the number of evaluation metric values meaning that problems can arise close to edges of the image data.

c) Mathematical sub-sample estimation using evaluation metric values also uses the smoothness of the surface of the evaluation metric values. Fitting a function, e.g. cosine or parabola, to three or more of the evaluation metric values (the extreme value and one situated on each side of it). By analytical solving of the function for its local extreme point, the sub-sample position can be found. However, it has been shown that fitting a function to a set of data is likely to produce incorrect results as the fitted function will not match the true curve of the fitted data possibly causing bias in the estimations [54]. Direct calculation of the sub-sample position can be achieved by e.g. grid slope interpolation [55] which were used in Papers II and III.

5. Motion estimation in cine loops – challenges and complexity

The cine loops used for evaluating motion estimation methods can originate from three sources (Figure 5): *in silico* – simulated in a computer, phantom – physical object with a likeness of tissue scanned with an ultrasound machine, and *in vivo* – ultrasound scans of living volunteers.

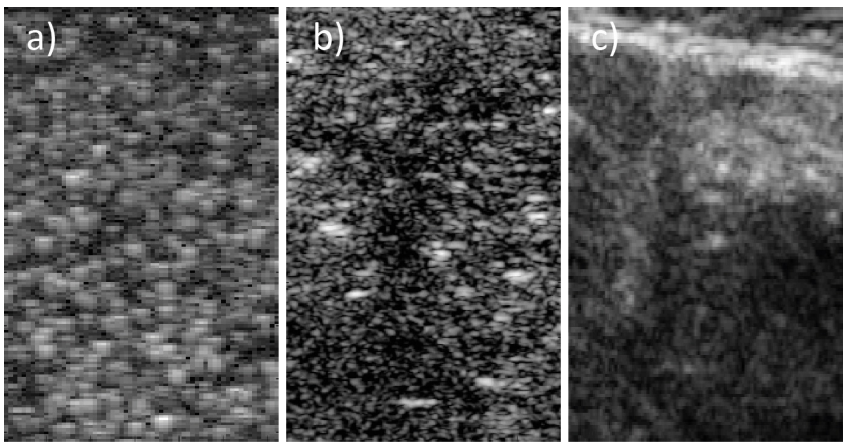

Figure 5. Examples of ultrasound images from the three sources: a) *in silico*, b) phantom, and c) *in vivo*. Each part of the image shows an area 20 x 15 mm. Parts of figure can be found in Paper III.

5.1 *In silico*

The first step of testing a new motion estimation method is in many cases to apply the method to image data simulated in a computer. A number of packages can be found on the internet, e.g. Field II [56, 57] and k-Wave [58, 59], and many more exist in various research labs around the world. The computers of today allow simulations to be calculated in a reasonable amount of time with increasingly accurate ultrasound models both concerning the physics and depicted physiology. Although the resulting cine loops will differ somewhat from those downloaded from an ultrasound machine, the benefits far outweigh the drawback in the initial test phase. As the user controls every step from the position of the scatterers of the simulated object, through the sampling of the data in the elements, to the beamforming, the image data can be fully controlled. As the motion of the scatterers in the simulated model is set by the user, the difference between the motion

estimations and the ground truth is more accurately known than when using phantom or *in vivo* data.

5.2 Phantoms

The use of phantoms as objects in an ultrasound investigation bridges *in silico* and *in vivo* data. *Ex vivo* investigations of tissue has in this thesis been classified as phantom studies. A number of substances with characteristics resembling human tissue, e.g. acoustic impedance, speed of sound, and absorption, are available. It is also possible to mold several of the substances, e.g. agar/gelatin and polyvinyl alcohol (PVA), for a desired form of the phantom. Having the phantom in a known situation gives a good control of its position at the time of the sampling of the ultrasound images. Also, the ultrasound machine used when sampling the phantom ultrasound data, are in most cases planned to be used when sampling *in vivo* data. Thus the resulting image data can resemble an *in vivo* measurement more than *in silico* data. Although the use of mechanical and robotic set-ups gives good control of the position of the phantom, the true position of the different parts of a phantom is not known as accurately as in the *in silico* data. It can also be very hard to manufacture phantoms in which complicated motions occur.

5.3 *In vivo*

The goal of developing a new ultrasound application is often research *in vivo*. Ultrasound cine loops with *in vivo* movements is, however, a rather difficult media in which to make motion estimations given the amount of absorption, noise, scattering, and multiple reflection which all decreases the image quality and disturbs the motion estimations.

A common problem during *in vivo* ultrasound investigations is out-of-plane movement. All image modalities have a field-of-view in which an object can be viewed. A 2D ultrasound investigation samples the image data with a certain elevation thickness with disrespect to the direction of an observed 3D-motion. Thus, great care has to be taken in order to capture a motion along a line fully within the image-plane. An angle between the image-plane and the motion will result in a velocity component perpendicular to the image-plane which will be unknown and, many times, not readily apparent. In some instances, the structure of the investigated tissue can be an indicator of out-of-plane movement, e.g. when investigating the arterial wall of the common carotid artery in a view parallel to the surface of the transducer, where the intima-media complex should be visible along the entire artery. Conducting motion estimations in the presence of an out-of-plane movement will result in an underestimation of the real physiological movement.

Also, if tracking with a Lagrangian viewpoint, it is possible that the interesting volume of tissue will move out of the ultrasound image-plane, and, thus, cannot be tracked. When investigating non-linear movements it might not be possible to avoid out-of-plane movement when sampling 2D cine loops. A modern solution is to sample 3D cine loops to better capture the movement.

The wish to have the best possible image quality can be a problem when estimating motion using *in vivo* cine loops. Although the use of persistence gives improved image quality when sampling ultrasound cine loops, it is also likely to blur the information needed for motion estimation, and will likely obstruct any attempts of motion estimation using block-matching. Also the use of multiple points of focus can cause problems by reducing the sampled frame rate to a degree where motion estimation becomes problematic.

The main difficulty of using *in vivo* data when testing a motion estimation method is, however, a reduced knowledge of the true motion in a cine loop. The "true" motion might be obtained using another image modality, e.g. magnetic resonance imaging, or by motion estimation in the same cine loop using an existing motion estimation method, or using (echogenic) beads surgically positioned *in vivo* [60, 61]. Ethical considerations will of course arise and the inserted object can both reduce the quality of the ultrasound images and disturb the tissue motion.

6. Arterial wall movement

Cardiovascular diseases are the leading causes of death worldwide [62]. A wish to better understand and predict diseases in the cardiovascular system has been a driving force for research of the cardiovascular system. The arterial wall consists of the tunica intima (the innermost layer), the tunica media (the middle layer), and the tunica adventitia (the outer wall). The intima is a sheet of flat endothelial cells resting on a thin layer of connective tissue. The endothelial layer is the main barrier to plasma proteins; further, it secretes many vasoactive products. Finally, it is mechanically weak. The tunica media supplies mechanical strength and contractile power. It consists of spindle-shaped, smooth muscle cells embedded in a matrix of elastin and collagen fibres. Sheets of elastin mark each boundary of the tunica media. The tunica adventitia is a connective tissue sheath with no distinct outer border. It serves to tether the vessel loosely in place. The adventitia consists of longitudinally oriented collagen and elastic fibres. The adventitia of the larger arteries contains small blood vessels, the *vasa vasorum* (literally "vessels of vessels"), and in the largest arteries these penetrate into the outer tunica media as well. Their task is to nourish the thick tunica media of the large vessels [63]. An established way to characterize the arterial wall using ultrasound is to measure the thickness of the two inner layers – the intima-media thickness [64]. The typical double-line pattern in ultrasonic images arising from the lumen-intima and media-adventitia boundaries can be used to measure the intima-media thickness either manually using calipers or automatically [65-69]. The knowledge that the arterial wall has a radial movement connected to the pulsation of the blood has been known for a long time and the radial motion, i.e. the diameter change of the artery, has been investigated since the 1970th using ultrasound. The diameter change has been measure in 1D and 2D RF-data [70-73], and using B-mode [68, 74-76].Another widely used measure is pulse wave velocity [22, 77-79] as it gives an indication of the stiffness of the vessel wall [80]. The finding of a longitudinal movement of the arterial wall of the same magnitude as the diameter change was first presented by our group [81] in 2002. Since the discovery of the longitudinal movement of the arterial wall, several papers have been published elaborating on and confirming not only the presence of a longitudinal vessel wall movement in large arteries, but also a longitudinal shearing within the vessel wall; the intima-media complex (the vessel wall layers closest to the lumen) of the carotid artery showing a larger movement than the adventitial layer (the outer vessel wall layer) [82, 83]. Other studies have indicated a possible relation between the maximal amplitude of the longitudinal movement of the common carotid artery wall and risk factors for vascular disease [84]. It is, however, of interest,

to not only study the maximal amplitude of longitudinal movement, but also the complex bidirectional multiphasic pattern of the longitudinal movement. It is possible that also the pattern of the longitudinal movement can be of predictable value (Paper IV).

The largest longitudinal movements of the common carotid artery have been observed in the intima-media complex. Thus, it is likely in these layers that a potential change of the magnitude and/or pattern of the longitudinal movement in a patient can be detected first. Considering that the intima-media complex is thin, has a marked radial curvature, and has a 3-dimensional motion pattern in Cartesian coordinates (radial plus longitudinal movement in cylindrical coordinates), acquiring cine loops of sufficient image quality is problematic. A precise positioning of the transducer is necessary in order to minimize the out of plane movement of the arterial wall. Even with a precise positioning of the transducer it can be difficult to visualize the near vessel wall (closest to the transducer) due to the clutter produced by the tissue.

In earlier investigations [83, 85], three distinct bi-directional phases of the longitudinal movement pattern were identified (Figure 6). The figure shows that an antegrade movement (along the direction of blood flow) can be observed in early systole, followed by a large distinct retrograde movement (opposite the direction of blood-flow) during late systole, and a second antegrade movement in diastole followed by a gradual return to the initial position. The pattern of the radial movement of the arterial wall, the distension, is caused by pressure waves [86]. The mechanisms underlying the different phases of the longitudinal movement is, however, mainly unknown, and it is likely to involve several factors. One hypothesis is that blood flow shear stress, acting along arteries, is one of the forces underlying the longitudinal movement. However, 1) this force is too small compared to the longitudinal elasticity of the arterial wall [87] and 2) in studies on the porcine artery it has been shown that a marked increase in the longitudinal movement can take place independently of wall shear stress from the blood flow [88]. It has been suggested that the retrograde phase of the longitudinal movement is caused by the motion of the heart. It is well known that the heart moves towards the apex in systole [89, 90]. If that suggestion is correct, then a gender specific difference of the longitudinal movement pattern could exist in elderly cohorts due to possible differences in the stretching of the ascending aorta [91]. It has also been shown that significant longitudinal movement can be estimated in a non-straight phantom with pulsating flow [92] suggesting that the blood pressure can influence the longitudinal movement. If the direct pulse wave during systole affects the longitudinal movement, surely reflected waves in the arterial system can do so too.

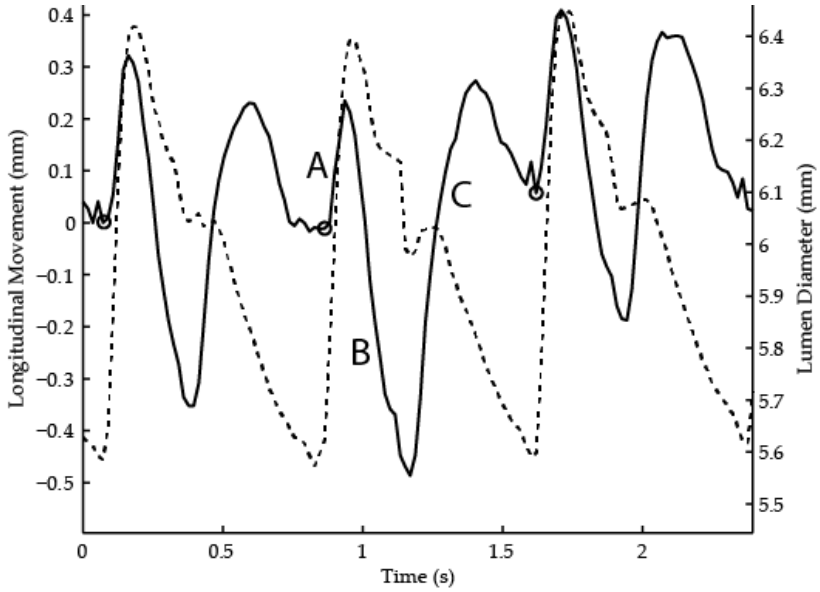

Figure 6. Longitudinal movement (solid) of the intima-media complex of the far wall of the common carotid artery and the corresponding diameter change (dashed) of a 28-year-old woman. The small circles mark the onset of an antegrade movement (along the direction of the blood flow) in early systole (Phase A). It is followed by a large distinct retrograde movement (against the direction of the blood-flow) during
Figure 6. Longitudinal movement (solid) of the intima-media complex of the far wall of the common carotid artery and the corresponding diameter change (dashed) of a 28-year-old woman. The small circles mark the onset of an antegrade movement (along the direction of the blood flow) in early systole (Phase A). It is followed by a large distinct retrograde movement (against the direction of the blood-flow) during late systole (Phase B) and a second antegrade movement in diastole (Phase C), followed by a gradual return to the initial position. Figure originally from Paper IV.

7. Included papers

7.1 Paper I

This paper investigated the effect of adding one extra kernel when estimating motion (Figure 7). Investigation of the motion estimations made using a sparse block-matching method showed that the length of most of the errors were one sample or less. Averaging the positions of the motion estimations using the sparse block-matching method and a FS method with a 3x3 sample search region was believed to improve the tracking accuracy with only a minor increase in calculation time.

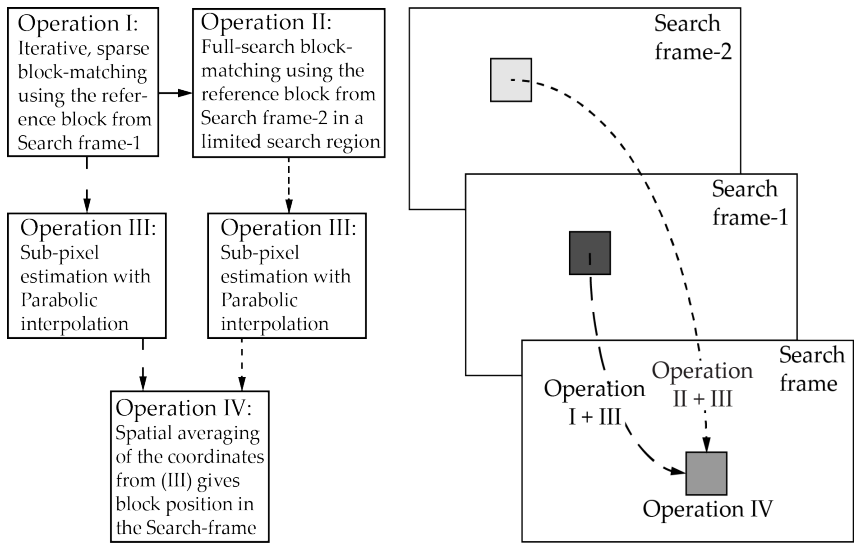

Figure 7. Tracking scheme for use of an extra kernel. Figure originally from Paper I.

In silico and phantom cine loops were used to evaluate the performance of an extra kernel. The results showed that tracking accuracy improved (mean = 48%, $p < 0.005$ [in silico]; mean = 43%, $p < 0.01$ [phantom]) compared to not using the extra kernel. As mentioned in 4.1.1, larger kernel size results in a general increase of tracking accuracy. Thus an increased tracking accuracy when using an extra kernel could be used to "buy" the use of a smaller kernel size without reduction in the tracking accuracy compared to not using an extra kernel. Using *in vivo* cine loops of the common carotid artery where the longitudinal movement of the arterial wall was estimated, an optimization for tracking accuracy were made using the sparse

block-matching method both with and without use of an extra kernel. With maintained tracking accuracy, a reduction (mean = 19%, $p < 0.01$) in kernel size were achieved.

It was shown that either an increased tracking accuracy or a decreased kernel size could be achieved with the use of an extra kernel which prove the contradiction between kernel size and tracking accuracy. Though the use of an extra kernel added to a basic motion estimation method clearly improve the tracking accuracy, the use of a biased sub-sample estimation method can concern the reader. But it is believed that the improved tracking accuracy comes from both the use of an extra kernel and the averaging of the two estimated positions. In worst case the averaging of the two estimated positions will result in the largest bias being kept and in best case the biases will be removed.

7.2 Paper II

This paper investigated the motion estimation performance of eight sub-sample methods when used in combination with three different evaluation metric methods. When the performance of a sub-sample estimation method is presented, it is normally investigated using only one evaluation metric method. However, as the shape of a theoretical surface (Figure 4) of evaluation metric values will differ between methods, the estimation errors of a sub-sample method were hypothesized to be affected. The aim of this paper was to investigate the performance of sub-sample estimation methods of the three groups presented in 4.5 using three different evaluation metric methods.

The investigation used simulated cine loops depicting a block moving in the lateral direction with a constant velocity. The results showed that the used evaluation metric method affected the motion estimation performance of the sub-sample estimation methods (Figure 8). The effect on the motion estimation performance varied with the sub-sample estimation method and one or several performance values of were affected: mean estimation error, standard deviation of estimation error, and calculation time. This indicates that a reported tracking performance for a sub-pixel estimation method can be significantly different when combined with another evaluation metric.

Though the main purpose of the evaluation metric method is to find the block most similar to the kernel, the shape of the evaluation metric values for all blocks in a region will influence both the used search methodology and the sub-sample estimation method. It should be clear that some sub-sample estimation methods are more specifically developed for use with one evaluation metric method than others. A test is thus required if only a part of a published method is used, i.e. it should always be tested as the images in which motion estimations are conducted affects the performance of a motion estimation method (author's opinion).

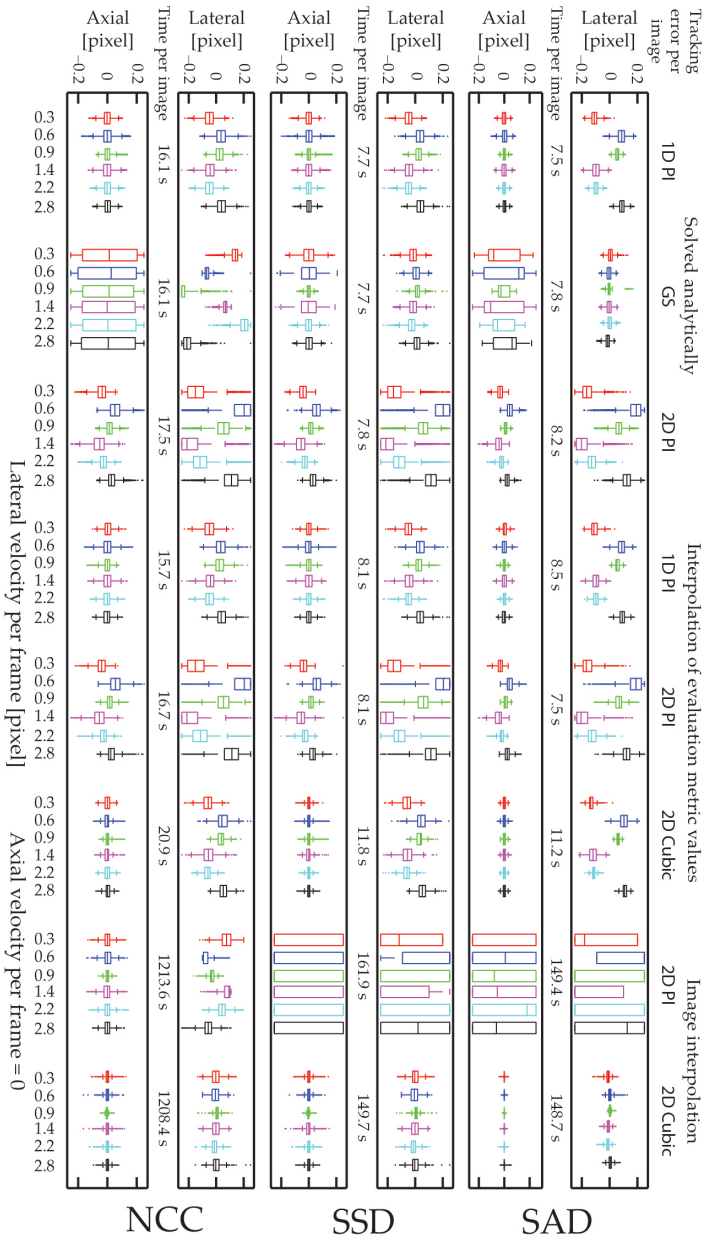

Figure 8. Tracking error per image of the motion estimation performed on the in silico cine loops against the set movement per image of the cine loops. The boxes indicate the lower and upper quartiles and the median. The bar line indicate 99% of the values. Outliers are indicated as points. Each box is based on 4,900 estimations explaining the seemingly large numbers of outliers. No error larger than 0.25 pixels is shown but they were part of all the statistics. Figure originally from Paper II.

7.3 Paper III

This paper investigated the effect of combining two published sub-sample estimation methods (Figure 9). Parabolic sub-sample interpolation for 2D block-matching motion estimation is computationally efficient. However, it is well known that the parabolic interpolation in the range of y – 0.5 to y + 0.5 samples gives a biased motion estimate with a maximum bias for displacements of y ± 0.25 samples (y = 0, 1, …) (Figure 9). Grid slope sub-sample interpolation is less biased, but it shows large variability for displacements close to y.0. The proposed solution is to combine these sub-sample methods using a threshold to determine when to use which method. The threshold were determined to ±0.15 samples using motion estimations in phantom cine loops. Hence the new method GS15PI.

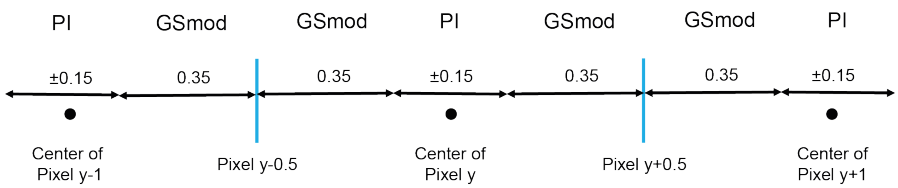

Figure 9. A representation of which interpolation method to use where for GS15PI. In this figure y is any sample position, PI is parabolic interpolation, and GSmod is our modified grid slope interpolation.

The new method was compared to three sub-sample interpolation methods: sub-sample interpolation of the image, parabolic sub-sample interpolation, and grid slope sub-sample interpolation. The evaluation used methods sampled *in silico*, on phantoms, and *in vivo*. In order to compare the sub-sample methods in an as objective manner as possible, the *in vivo* evaluation was limited to the longitudinal movement of the arterial vessel wall of the common carotid artery of 21 healthy volunteers. Only the retrograde motion, against the blood flow, was used in the comparison as it is the most distinct and regular phase of the motion pattern at the measured site. Evaluated on simulated and phantom cine loop, GS15PI reduced on average the absolute sub-sample estimation errors by 14, 8, and 24%, respectively. The drawbacks of the parabolic and modified grid slope sub-sample estimation methods were reduced in GS15PI as predicted (Figure 10). When evaluated *in vivo*, the motion estimations using parabolic and grid slope sub-sample interpolation and GS15PI resulted in coefficient of variation values of 6.9, 7.5, and 6.8%, respectively.

It was expected that the total motion estimations should be smaller when using RF data compared to using B-mode data. However, the results in this paper were not conclusive and the results indicate that both RF data and B-mode data can be

preferable. As the trends found indicate similar behavior for all sub-sample methods, it can be suspected that the sources of the used data are the cause of this inconsistency.

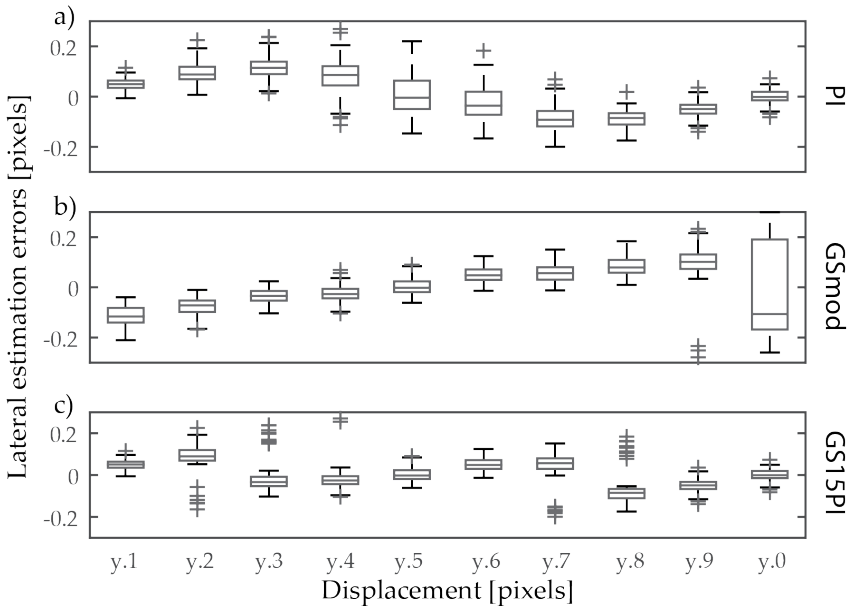

Figure 10. Comparison of the bias of three sub-sample estimations methods. In this figure, y is a natural number. Figure originally from Paper III.

7.4 Paper IV

This paper investigated the longitudinal movement patterns of the intima-media complex of the wall of the right common carotid artery in 135 healthy volunteers. Although the knowledge and understanding of the longitudinal movement pattern of the arterial wall have increased in the last decade, the physiology behind the pattern is not yet understood. Further, putative changes in the longitudinal movements with aging have not been defined. Our group has previously shown that the movement pattern of the common carotid artery for an individual is stable over a four-month period [93] and that the pattern of movement in young healthy subjects can markedly differ, also between subjects of the same age and gender. Three major phases of movement have previously been identified [93]. The large cohort of healthy volunteers in this study included subjects of a wide range of age and gave the possibility to define changes in the longitudinal movement in the normal aging process of the arterial system.

In this study we defined two phases of longitudinal movement of the common carotid artery that have not previously been described. The first additional phase was rapid, retrograde and started just before end-diastole, and ended approximately at the time of the start of systole (Figure 11a). This phase was most prominent in volunteers 50-65 years of age. The second additional phase was antegrade and occurred during, or directly after the dicrotic notch was observed in the diameter curve (Figure 11b). This phase was not distinct in all individuals; especially not in the young. The size of the phase ranged from only a change in velocity of the retrograde phase to a distinct antegrade motion in older individuals. The healthy individuals could also be divided into five different groups based on the resulting pattern of the longitudinal movement. The results in this paper suggest a relationship between the movement pattern and aging of an individual, or perhaps rather the aging of the cardiovascular system. All individuals were without known health problem, and the results can be useful both for comparison in studies of individuals with a known disease, and serve as a base for further studies of the physiology of the vascular system in healthy individuals.

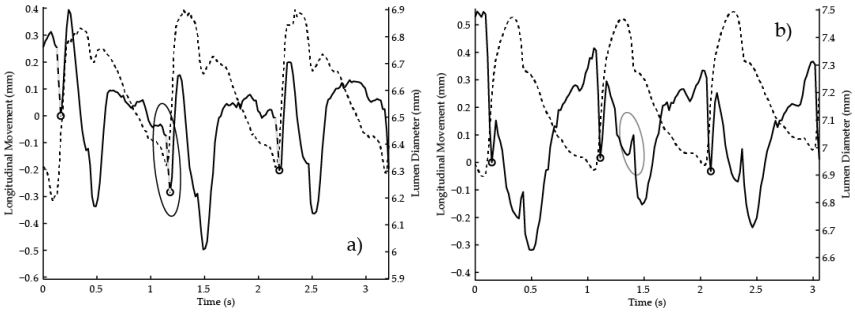

Figure 11. Longitudinal movement (solid) of the intima-media complex of the far wall of the common carotid artery, and corresponding diameter change (dashed). The small circles mark the onset of an antegrade movement in early systole. a) Shows a 53-year-old male with a distinct large retrograde movement (marked by a large oval) just before end-diastole. b) Shows a 60-year-old female with a distinct antegrade movement (marked by a large oval) at the time when the dicrotic notch is observed in the diameter change curve. For longitudinal movement, a positive deflection denotes movement in the direction of blood flow.

7.5 Paper V

This paper investigated a new motion tracking scheme for improved motion estimations with a Lagrangian viewpoint in high frame rate cine loops. Cine loops sampled at high frame rate are increasingly used and interest of estimating motion in them is high. One reoccurring problem using *in vivo* measurements is the short movement between consecutive images due to the high frame rate and relative slow movements, e.g. a frame rate of 1300 s^{-1}, motion velocity of 2 mm/s, and a sample density in the direction of movement of 10 mm^{-1} results in a displacement per frame of 0.015 samples. For such short motion, it is very likely that the relative motion estimation errors will be high if using a block-matching method. If a Lagrangian viewpoint is used for the motion estimations, the accuracy of the estimated positions will most likely decrease with the number of consecutive images as the errors of the estimated positions will accumulate from previous estimations. We propose to perform the motion estimations iteratively and in the first iteration take rather large steps between the used images. The positions in the images between the first iteration will then be estimated using the previous iterations (Figure 12). The estimations will have three benefits: in the early iterations, the motion between used images will be larger and the relative error small, the motion estimations will be based on two independent kernels in all images, and the accumulated errors for the estimated position will be smaller due to less number of estimations needed before reaching the image of interest.

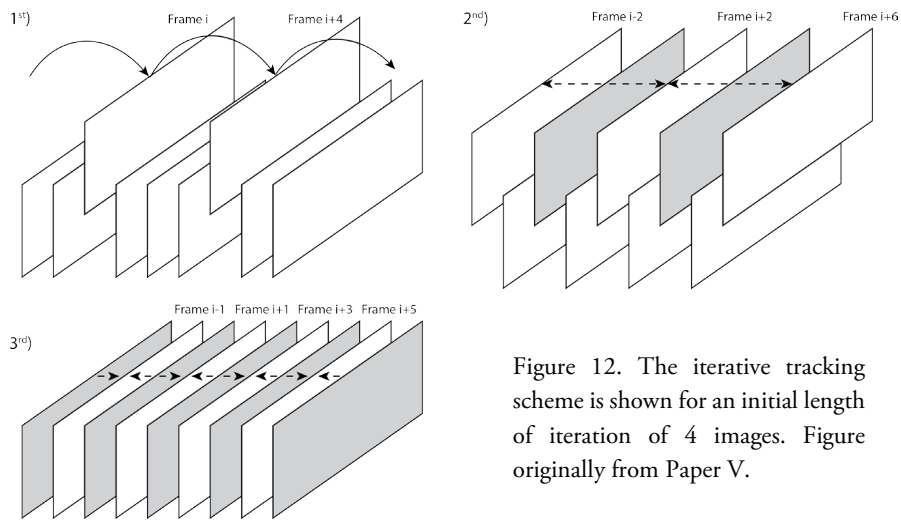

Figure 12. The iterative tracking scheme is shown for an initial length of iteration of 4 images. Figure originally from Paper V.

The new tracking scheme was tested on phantom cine loops sampled at 1302 frames per second and beamformed using three different methods: delay-and-sum, phase correlation imaging, and transverse oscillation. The phantom were scanned with two transducers with 100 and 200 µm pitch, i.e. the distance between the center of the elements in the transducer. Comparisons were made both for estimations of the velocity and the total displacement of the phantom. Motion estimations in cine loops sampled at a low frame rate were conducted for comparison.

The iterative motion estimation scheme works well with the used block-matching method (Figure 13). Longer initial iteration length resulted in smaller standard deviation in the estimates than the shortest initial iteration lengths. It also resulted in mean estimation errors closer to zero than using the medium initial iteration lengths. Neither the pitch of the transducer or beamforming method had a major influence on the estimation errors. The size of the pitch of the transducer had much larger influence when using a low frame rate sampling.

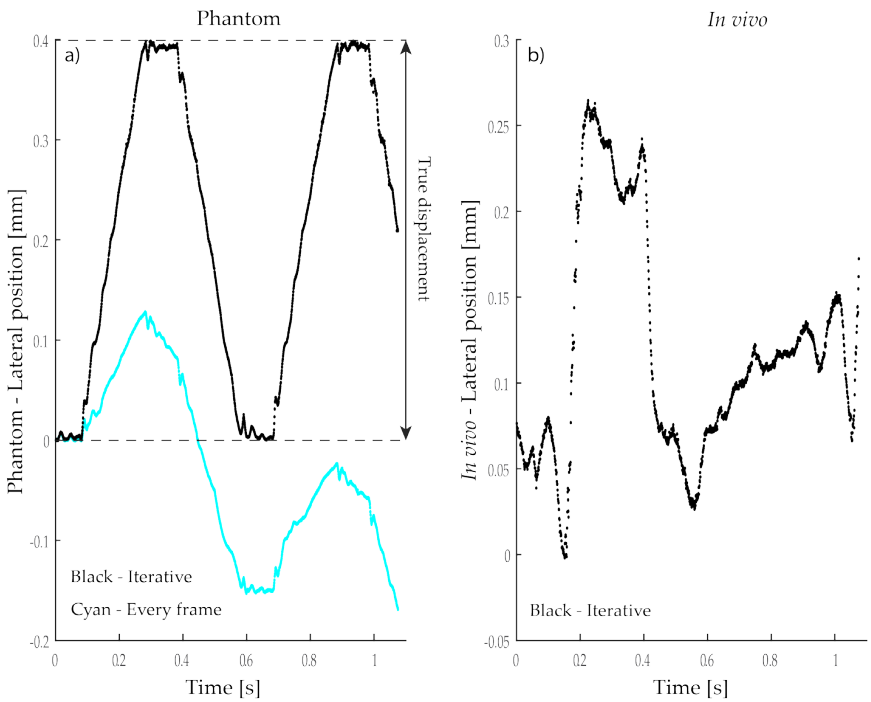

Figure 13. Estimated lateral positions using the proposed iterative tracking scheme shown in black. The same motion estimation method were used for the cyan line but without the iterations. Figure originally from Paper V.

The results in Paper V showed that our hypothesis, that block-matching methods prefer longer movements, is true. It is also clear from the figures that the method still could estimate small movements (Figure 13). Please note, that the small oscillations observed in Figure 13a, when the phantom had reached full displacement, have been confirmed to be true. The results also indicate that the size of the pitch only gave a limited effect on the motion estimation errors when using high frame rate images. This could be compared to the reduction of the motion estimation errors when using a smaller pitch and the low frame rate images. This indicates that the use of a focus during transmit is the underlying effect on the motion estimation errors when using different sizes of pitch. Although the beamforming methods clearly affects the images visually, an evaluation metric method will act as a strong filter and remove most of the effect of the beamforming method. Thus the accuracy of motion estimation using block-matching is more affected by the shape of the surface of evaluation metric values than the samples in the image. This is clearly shown by the minor differences in tracking accuracy for the beamforming methods.

8. Discussion

The research in this thesis include three innovative methods presented in Papers I, III, and V. One common characteristic is that they use two sources of information to improve the performance of motion estimations: in Paper I two motion estimations are performed using two different kernels from sequential images; in Paper III the sub-sample estimation of one method is used with a threshold to determine whether a second sub-sample estimation method should be used instead; and in Paper V two motion estimations are performed using two different kernels from the anteroposterior images which have opposite relative velocities. Using two, or more, different sources of information during motion estimation may be used in other situations; e.g. can the use of RF data and B-mode data for the same kernel be beneficious? Preferably the used methods should be as independent as possible. However, all methods will be using the ultrasound images as their source of data which implies that total independence can never be achieved. The use of two estimation methods can easily be confused with use of *a priori* information and depending on the use of the *a priori* information they can be the same. The idea when using multiple estimation methods, is that the strengths of the methods should be used to remove any weakness.

The change from using data sampled in two dimensions to the use of data sampled in three dimensions cause only minor changes in many methods of motion estimation. The major influence of using 3D image data is the time needed to sample the data in each image as a relatively slow sampling time can result in shearing of the data as the depicted objects will move during sampling. If sufficiently high sampling rate can be achieved, the use of 3D images will very likely increase our understanding of the studied objects.

That the image quality affects the motion estimations performed is clear. The quality will be affected by both the used ultrasound equipment and the settings used during acquisition. This introduces problems when comparing methods for motion estimation. Implementing another researchers motion estimation methods can be problematic as researchers often optimizes their methods without reporting the exact procedure, and that optimization is often depending on the used cine loops. Trying the alternative, to reproduce the cine loops of other researchers, will also be difficult. *In silico* cine loops can be rather well recreated when simulated by someone else though randomness entered in scatter location and strength as well as any added noise can have a small effect. The main problem using *in silico* cine loops are that many authors are rather lax in detailing the settings when simulating their cine

loops. Phantom measurements will be influenced by both the setting on the ultrasound machine and the phantom. Though the used equipment is rather well described, descriptions of the used settings on ultrasound machine are mostly rather sparse except on the used frame rate. Sometimes, facts about the used phantom are also missing. Significant differences can be observed between the *in vivo* cine loops used by different research groups. Not only are the settings mostly unknown but, most important, each individual is different. Thus motion estimations conducted in two individuals are likely to result in slightly varying results. When developing a new motion estimation method the available cine loops are used; both for developing and testing the method. It is then possible to develop a method that works very well with the cine loops in the testing but when testing the method on other cine loops the motion estimation errors can differ drastically. A solution to this problem, and a way for easier comparison of different motions estimation methods, would be an open database or competitions [94] with cine loops depicting different object of varying complexity. This could result in better and more objective comparisons with agreed upon evaluation metrics.

One aim of Paper II was to evaluate the effect on the motion estimation errors for a given sub-sample estimation method when the evaluation metric method was changed. The reason for changes in the motion estimation errors is different for the three types of sub-sample estimation methods:

a. Interpolation of the data points; most if not all effects of the evaluation metric method arise during search for the extreme point. The different evaluation metric methods give slightly different tracking accuracy with the same search method (Figure 8).
b. Interpolation of evaluation metric values; any effects depends on the sub-sample estimation method. As the theoretical curve or surface of the evaluation metric values differs between the evaluation metric methods, the sub-sample estimation methods ability to accurately mimic the theoretical curve or surface of the current evaluation metric method will determine the accuracy of the interpolations and the accuracy can thus differ between evaluation metric methods. However, the fit of the function in amplitude is not as important as the spatial fit, i.e. the extreme point should be at the correct position.
c. Analytically solving the min/max problem for the evaluation metric values; again the fit between the theoretical curve and the used function determines the estimation accuracy. However, the fit of the function in amplitude is not as important as the spatial fit, i.e. the extreme point should be at the correct position.

Out of plane movement is an insidious problem with ultrasound when measuring motion and care has to be taken to position the ultrasound probe so the investigated motion is taking place in the image plane. The problem is that unless the investigated object contains a surface or line that is known to be parallel with the investigated motion it is very hard to detect a slow out of plane motion and if a lot of speckle decorrelation exists, even a fast out-of-plane motion can be hard to detect. It has been suggested to use the correlation of the speckle before and after movement [95] but that is mainly valid if no in-plane motion exists as the changes in the correlation values due to the in-plane values are in the same order or larger than the changes caused by the out of plane motion (Figure 14). Another problem when measuring *in vivo* is the existence of non-linear motions, especially if the motion is not limited to a plane. In this case, the best solution for the user is to find the position for the transducer that minimize the out of plane movement. In worst case the entire motion can only be piecewise estimated with reasonable out of plane movements. In the future, the use of 3D ultrasound image is likely to solve this problem entirely.

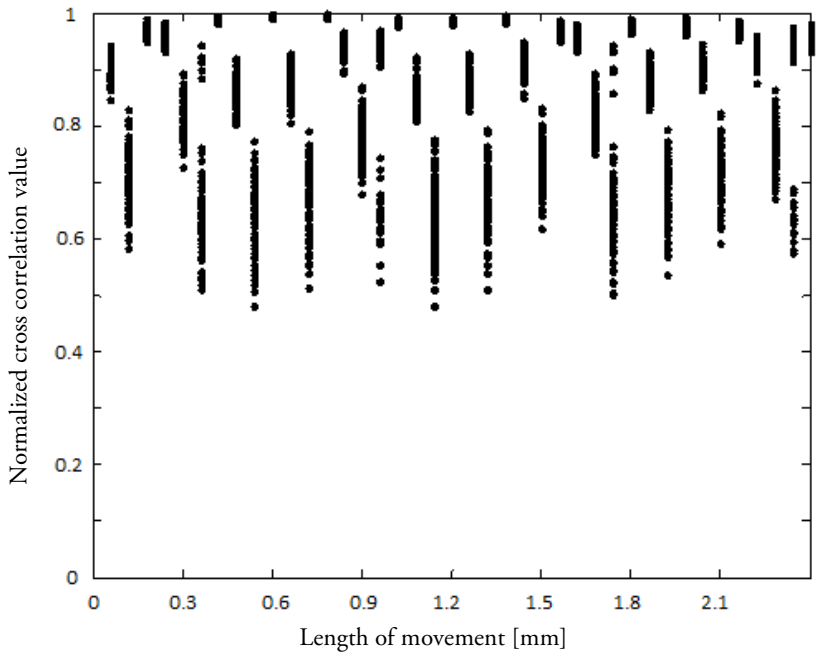

Figure 14. The evaluation metric values using normalized cross correlation for 80 kernels when moving a phantom in the lateral direction without out of plane motion. Please note that the motion estimations for all movements were correct at pixel level.

9. Summary

This thesis has presented new block-matching motion estimation methods developed for generic *in vivo* use. The methods have been evaluated and compared to existing methods *in silico*, on phantoms, and *in vivo*. Our findings include:

- The use of an extra kernel from an earlier frame – which was shown to reduce the estimation errors while maintaining the kernel size, or to decrease the kernel size while maintaining the level of the estimation errors. Also, a possible increase of usability has been observed *in vivo*, although not quantified, compared to our previous methods.
- A combined sub-sample motion estimation method – which combines two sub-sample estimation methods and reduces the negative attributes of the two combined sub-sample estimation methods while retaining their positive attributes.
- An iterative motion estimation scheme for use in high frame rate cine loops – the tracking scheme was shown to give accurate estimations with a Lagrangian viewpoint over 1024 images in Paper V but longer (~6000 images) cine loops have successfully been used (unpublished data).
- The first two methods have been used to extend our knowledge of the longitudinal movement of the arterial wall *in vivo*. The combined methods performed well; motion estimations were acquired in all valid subjects. Three previously movement phases and two additional movement phases were investigated. The results suggest a relationship between the longitudinal movement pattern and aging of an individual. Cine loops at a low (~50 Hz) frame rate were used but we now have the tools to investigate the longitudinal movement at a high (~1500 Hz) frame rate.

This thesis thus present and evaluate refined methods to measure vascular function through the estimation of longitudinal movement.

10. Future considerations

There are two major paths leading from this thesis: one path leads towards improved methods for motion estimation using ultrasound data; and the other path leads towards a better understanding of the human physiology. In most of the work, SAD has been used for estimating similarity. The benefits of SAD include low calculation times and high accuracy of motion estimations using B-mode data. The drawback is that SAD, in my experience, gives a rather low accuracy when estimating motions using RF data. An equally fast method but with a higher accuracy could be beneficial. Although GS15PI reduced the bias of the two used sub-sample methods, the break point of 0.15 was tested on one series of cine loops and might not be optimal. Also, replacing one of the sub-sample estimation methods with another method could further improve of the results. On the physiological path, one step has already been taken in Paper IV. A much larger material of motion estimations from both healthy individuals and from individuals with cardiovascular diseases and cardiovascular risk factors, are needed to determine if the magnitude of the longitudinal movement and/or the movement pattern can be used as a biomarker for cardiovascular disease. However, the methods presented should not only be limited to studies of the cardiovascular system as they are universal tools for motion estimations in B-mode or pixelated image data.

When it comes to investigating the longitudinal vessel wall movement of the common carotid artery, the next step could be 3D volumes of the artery at a frame rate of at least 50 Hz. That would require a 2D-array ultrasound transducer, center frequency 7-12 MHz, with a field of view large enough to see the full movement of the artery during a full heart cycle, e.g. a cube with sides at least 2 mm long. In order to avoid shearing of the ultrasound images, plane wave imaging is probably needed but then the image quality also needs to be improved. With this set-up, the intima-media complex should be visible in every ultrasound investigation and it would be much easier to collect image data with sufficient image quality for accurate motion estimations.

It is 15 years since the first measurements were presented on longitudinal movement. Considering that most of the measurements have been conducted on healthy volunteers the meaning of the different phases of the longitudinal movement in a health perspective is still difficult to see today. With the tools investigated in this thesis, it is now time to approach the clinical world and collect data from patients to try to see if these phases can be used as indicators and hopefully early indicator of diseases. Such work has already been started, e.g. in a European

project denoted SUMMIT ("Surrogate markers for micro- and macro-vascular hard endpoints for innovative diabetes tools"). However, the need for high quality *in vivo* cine loops of both healthy and diseased individuals are large and the motion estimation methods of today are still not capable of estimating motion in all collected cine loops. Although the research in this thesis show an increased robustness in the motion estimations and will be valuable tools in present research, it is believed that further improvements will be needed in the future. Thus, research should be made to both increase the performance of the motion estimation methods and to increase the usability of the cine loops by signal processing of the image data.

Although we in Paper V found that the beamforming method had a minor influence on the motion estimation errors when using our iterative block-matching tracking scheme, it is believed that the beamforming method has an important role to fill: to visualize the echoes in the ultrasound images. The image quality of cine loops from a commercial ultrasound machine and the high frame rate cine loops used in Paper V differs a lot and the reduced image quality impedes accurate motion estimations in the high frame rate images. Improving the image quality is thus necessary in order to get good motion estimations *in vivo* high frame rate images.

11. References

[1] T. L. Szabo, *Diagnostic Ultrasound Imaging*: Academic Press Elsevier, 2004.

[2] *Diagnostic Ultrasound: Physics and Equipment*: Greenwich Medical Media Limited, 2003.

[3] D. W. Baker, "Pulsed ultrasonic Doppler blood-flow sensing," *IEEE Trans. Son. Ultrason.,* vol. SU-17, pp. 170-185, 1970.

[4] L. N. Bohs and G. E. Trahey, "A novel method for angle independent ultrasonic imaging of blood flow and tissue motion," *IEEE Trans. Biomed. Eng.,* vol. 38, pp. 280-286, 1991.

[5] O. Bonnefous and P. Pesqué, "Time domain formulation of pulse-Doppler ultrasound and blood velocity estimation by cross-correlation," *Ultrasonic Imaging,* vol. 8, pp. 73-85, 1986.

[6] P. G. de Jong, T. Arts, A. P. Hoeks, and R. S. Reneman, "Determination of tissue velocity by correlation interpolation of pulsed ultrasonic echo signals," *Ultrasonic Imaging,* vol. 12, pp. 84-98, 1990.

[7] J. Farron, T. Varghese, and D. G. Thelen, "Measurement of Tendon Strain During Muscle Twitch Contractions Using Ultrasound Elastography," *IEEE Trans. Ultrason. Ferroelectr. Freq. Control,* vol. 56, pp. 27-35, 2009.

[8] H. Kanai, H. Hasegawa, M. Ichiki, F. Tezuka, and Y. Koiwa, "Elasticity imaging of atheroma with transcutaneous ultrasound - preliminary study," *Circulation,* vol. 107, pp. 3018-3021, 2003.

[9] W. N. McDicken, G. R. Sutherland, C. M. Moran, and L. N. Gordon, "Colour Doppler velocity imaging of the myocardium," *Ultrasound Med. Biol.,* vol. 18, pp. 651-654, 1992.

[10] P. Tortoli, G. Bambi, and S. Ricci, "Accurate Doppler Angle Estimation for Vector Flow Measurements," *IEEE Trans. Ultrason. Ferroelectr. Freq. Control,* vol. 53, pp. 1425-1431, 2006.

[11] P. N. T. Wells, "A range gated ultrasonic Doppler system," *Med. Biol. Eng.,* vol. 7, pp. 641-652, 1969.

[12] J. Kirkhorn. (1999, 2017-03-24). Introduction to IQ-demodulation of RF-data.

[13] C. Bruneel, R. Torguet, K. M. Rouvaen, E. Bridoux, and B. Nongaillard, "Ultrafast echotomographic system using optical processing of ultrasonic signals," *Appl. Phys. Lett.,* vol. 30, pp. 371-373, 1977.

[14] L. Sandrin, S. Catheline, M. Tanter, X. Hennequin, and M. Fink, "Time-resolved pulsed elastography with ultrafast ultrasonic imaging," *Ultrasonic Imaging,* vol. 21, pp. 259-272, 1999.

[15] E. Tiran, T. Deffieux, M. Correia, D. Maresca, B.-F. Osmanski, L.-A. Sieu*, et al.*, "Multiplane wave imaging increases signal-to-noise ratio in ultrafast ultrasound imaging," *Physics in Medicine & Biology,* vol. 60, pp. 8549-8566, 2015.

[16] M. Tanter, J. Bercoff, L. Sandrin, and M. Fink, "Ultrafast Compound Imaging for 2-D Motion Vector Estimation: Application to Transient Elastography," *IEEE Trans. Ultrason. Ferroelectr. Freq. Control,* vol. 49, pp. 1363-1374, 2002.

[17] G. Montaldo, M. Tanter, J. Bercoff, N. Benech, and M. Fink, "Coherent plane-wave compounding for very high frame rate ultrasonography and transient elastography," *IEEE Trans. Ultrason. Ferroelectr. Freq. Control,* vol. 56, pp. 489-506, 2009.

[18] G. R. Lockwood, Talman, and S. S. Brunke, "Real-time 3D ultrasound imaging using sparse synthetic aperture beamforming," *IEEE Trans. Ultrason. Ferroelectr. Freq. Control,* vol. 45, pp. 980-988, 1998.

[19] S. I. Nikolov and J. A. Jensen, "In-vivo synthetic aperture flow imaging in medical ultrasound," *IEEE Trans. Ultrason. Ferroelectr. Freq. Control,* vol. 50, pp. 848-856, 2003.

[20] M. Couade, M. Pernot, C. Prada, E. Messas, J. Emmerich, P. Bruneval*, et al.*, "Quantitative assessment of arterial wall biomechanical properties using shear wave imaging," *Ultrasound in medicine & biology,* vol. 36, pp. 1662-1676, 2010.

[21] H. Hasegawa and H. Kanai, "Simultaneous imaging of artery-wall strain and blood flow by high frame rate acquisition of RF signals," *IEEE Trans. Ultrason. Ferroelectr. Freq. Control,* vol. 55, pp. 2626-2639, 2008.

[22] J. Vappou, J. W. Luo, and E. E. Konofagou, "Pulse wave imaging for noninvasive and quantitative measurement of arterial stiffness in vivo," *Am. J. Hypertens.,* vol. 23, pp. 393-398, 2010.

[23] J. Bercoff, G. Montaldo, T. Loupas, D. Savery, F. Meziere, M. Fink*, et al.*, "Ultrafast compound Doppler imaging: Providing full blood flow

characterization," *IEEE Trans. Ultrason. Ferroelectr. Freq. Control,* vol. 58, pp. 134-147, 2011.

[24] K. L. Hansen, J. Udesen, F. Gran, J. A. Jensen, and M. B. Nielsen, "In-vivo examples of flow patterns with the fast vector velocity ultrasound method," *Ultraschall Med.,* vol. 30, pp. 471-477, 2009.

[25] E. Mace, G. Montaldo, B.-F. Osmanski, I. Cohen, M. Fink, and M. Tanter, "Functional ultrasound imaging of the brain: Theory and basic principles," *IEEE Trans. Ultrason. Ferroelectr. Freq. Control,* vol. 60, pp. 492-506, 2013.

[26] D. F. Young, B. R. Munson, and T. H. Okiishi, *A Brief Introduction to Fluid Mechanics*, 3rd ed.: John Wiley & Sons, Inc., 2004.

[27] A. Wedel and D. Cremers, *Stereo Scene Flow for 3D Motion Analysis*: Springer-Verlag London, 2011.

[28] C. D. Kuglin and D. C. Hines, "The phase correlation image alignment method," *Proc. Int. Conf. Cybernetics and Society,* pp. 163-165, 1975.

[29] H. Foroosh, J. B. Zerubia, and M. Berthod, "Extension of Phase Correlation to Subpixel Registration," *IEEE Trans. Image Process.,* vol. 11, pp. 188-200, 2002.

[30] W. S. Hoge, "A Subspace Identification Extension to the Phase Correlation Method," *IEEE Trans. Med. Imag.,* vol. 22, pp. 277-280, 2003.

[31] Y. Keller and A. Averbuch, "A projection-based extension to phase correlation image alignment," *Signal Process,* vol. 87, pp. 124-133, 2007.

[32] P. Tortoli, G. Guidi, P. Berti, F. Guidi, and D. Righi, "An FFT-based flow profiler for high-resolution in vivo investigations," *Ultrasound Med. Biol.,* vol. 23, pp. 899-910, 1997.

[33] H. Kanai, M. Sato, Y. Koiwa, and N. Chubachi, "Transcutaneous Measurement and Spectrum Analysis of Heart Wall Vibrations," *IEEE Trans. Ultrason. Ferroelectr. Freq. Control,* vol. 43, pp. 791-810, 1996.

[34] M. Evertsson, M. Cinthio, S. Fredriksson, F. Olsson, H. W. Persson, and T. Jansson, "Frequency- and Phase-Sensitive Magnetomotive Ultrasound Imaging of Superparamagnetic Iron Oxide Nanoparticles," *IEEE Trans. Ultrason. Ferroelectr. Freq. Control,* vol. 60, pp. 481-491, 2013.

[35] A. Pesavento, C. Perrey, M. Krueger, and H. Ermert, "A time-efficient and accurate strain estimation concept for ultrasonic elastography using iterative phase zero estimation," *IEEE Trans. Ultrason. Ferroelectr. Freq. Control,* vol. 46, pp. 1057-1067, 1999.

[36] X. Chen, M. J. Zohdy, S. Y. Emelianov, and M. O'Donnell, "Lateral speckle tracking using synthetic lateral phase," *IEEE Trans. Ultrason. Ferroelectr. Freq. Control,* vol. 51, pp. 540-550, 2004.

[37] J. A. Jensen and P. Munk, "A new method for estimation of velocity vectors," *IEEE Trans. Ultrason. Ferroelectr. Freq. Control,* vol. 45, pp. 837-851, 1998.

[38] H. Liebgott, J. E. Wilhjelm, J. A. Jensen, D. Vray, and P. Delachartre, "PSF Dedicated to Estimation of Displacement Vectors for Tissue Elasticity Imaging with Ultrasound," *IEEE Trans. Ultrason. Ferroelectr. Freq. Control,* vol. 54, pp. 746-756, 2007.

[39] F. Varray and H. Liebgott, "An alternative method to classical beamforming for Transverse Oscillation Images: Application to Elastography," presented at the 2013 IEEE 10th International Symposium on Biomedical Imaging, San Francisco, 2013.

[40] E. Konofagou and J. Ophir, "A New Elastographic Method for Estimation and Imaging of Lateral Displacements, Lateral Strains, Corrected Axial Strains and Poisson's Ratios in Tissues," *Ultrasound Med. Biol.,* vol. 24, pp. 1183-1199, 1998.

[41] J. Ophir, I. Céspedes, H. Ponnekanti, Y. Yazdi, and X. Li, "Elastography: A Quantitative Method for Imaging the Elasticity of Biological Tissues," *Ultrasonic Imaging,* vol. 13, pp. 111-134, 1991.

[42] I. A. Hein and W. D. O'Brien, "Current Time-Domain Methods for Assessing Tissue Motion by Analysis from Reflected Ultrasound Echoes-A Review," *IEEE Trans. Ultrason. Ferroelectr. Freq. Control,* vol. 40, pp. 84-102, 1993.

[43] A. Gastounioti, S. Golemati, J. Stoitsis, and K. S. Nikita, "Comparison of Kalman-filter-based approaches for block matching in arterial wall motion analysis from B-mode ultrasound," *Meas. Sci. Technol.,* vol. 22, p. 114008, 2011.

[44] R. G. P. Lopata, M. M. Nillesen, H. H. G. Hansen, I. H. Gerrits, J. M. Thijssen, and C. L. de Korte, "Performance Evaluation of Methods for Two-Dimensional Displacement and Strain Estimation Using Ultrasound Radio Frequency Data," *Ultrasound Med. Biol.,* vol. 35, pp. 796-812, 2009.

[45] Y. Nie and K.-K. Ma, "Adaptive rood pattern search for fast block-matching motion estimation," *IEEE Trans. Image Process.,* vol. 11, pp. 1442-1449, 2002.

[46] R. G. Keys, "Cubic Convolution Interpolation for Digital Image Processing," *IEEE Trans. Acoust., Speech, Signal Process.,* vol. ASSP-29, pp. 1153-1160, 1981.

[47] G. Zahnd, M. Orkisz, A. Sérusclat, P. Moulin, and D. Vray, "Evaluation of a Kalman-based block matching method to assess the bi-dimensional motion of the carotid artery wall in B-mode ultrasound sequences," *Med. Image Anal.,* vol. 17, pp. 573-585, 2013.

[48] T. Koga, K. Iinuma, A. Hirano, Y. Iijima, and T. Ishiguro, "Motion–compensated interframe coding for video conferencing," *Proc. Nat. Telecom. Conf.,* pp. G.5.3.1-G.5.3.5, 1981.

[49] L. M. Po and W. C. Ma, "A novel four–step search algorithm for fast block motion estimation," *IEEE T. Circ. Syst. Vid,* vol. 6, pp. 313-317, 1996.

[50] A. Puri, H. M. Hang, and D. Schilling, "An efficient block–matching algorithm for motion–compensated coding," *Proc. IEEE Int. Conf. Acoustics, Speech, and Signal Processing,* vol. 12, pp. 1063-1066, 1987.

[51] C. Zhu, X. Lin, and L. P. Chau, "Hexagon–based search pattern for fast block motion estimation," *IEEE T. Circ. Syst. Vid,* vol. 12, pp. 349-355, 2002.

[52] F. Yeung, S. F. Levinson, and K. J. Parker, "Multilevel and Motion Model-Based Ultrasonic Speckle Tracking Algorithms - Ultrasonic imaging of tissue strain and elastic modulus in vivo," *Ultrasound Med. Biol.,* vol. 24, pp. 427-441, 1998.

[53] C.-H. Lin, M. C.-J. Lin, and Y.-N. Suna, "Ultrasound motion estimation using a hierarchical feature weighting algorithm," *Comput. Med. Imag. Grap.,* vol. 31, pp. 178-190, 2007.

[54] E. I. Cespedes, Y. Huang, J. Ophir, and S. Spratt, "Methods for Estimation of Subsample Time Delays of Digitized Echo Signals," *Ultrasonic Imaging,* vol. 17, pp. 142-171, 1995.

[55] B. J. Geiman, L. N. Bohs, M. E. Anderson, S. M. Breit, and G. E. Trahey, "A novel interpolation strategy for estimating subsample speckle motion," *Phys. Med. Biol.,* pp. 1541-1552, 2000.

[56] J. A. Jensen, "Field: A program for Simulating Ultrasound Systems," *Med. Biol. Eng. Comput.,* vol. 34, pp. 351-353, 1996.

[57] J. A. Jensen and N. B. Svendsen, "Calculation of pressure fields from arbitrarily shaped, apodized, and excited ultrasound transducers," *IEEE Trans. Ultrason. Ferroelectr. Freq. Control,* vol. 39, pp. 262-267, 1992.

[58] B. E. Treeby and B. T. Cox, "k-Wave: MATLAB toolbox for the simulation and reconstruction of photoacoustic wave-fields," *J. Biomed. Opt.,* vol. 15, 2010.

[59] B. E. Treeby, J. Jaros, A. P. Rendell, and B. T. Cox, "Modeling nonlinear ultrasound propagation in heterogeneous media with power law absorption using a k-space pseudospectral method," *J. Acoust. Soc. Am.,* vol. 131, pp. 4324-4336, 2012.

[60] E. Widman, K. Caidahl, B. Heyde, J. D'Hooge, and M. Larsson, "Ultrasound Speckle Tracking Strain Estimation of In Vivo Carotid Artery Plaque with In Vitro Sonomicrometry Validation," *Ultrasound Med. Biol.,* vol. 41, pp. 77-88, 2015.

[61] T. Toyoda, H. Baba, T. Akasaka, M. Akiyama, Y. Neishi, J. Tomita*, et al.*, "Assessment of Regional Myocardial Strain by a Novel Automated Tracking System from Digital Image Files," *J Am Soc Echocardiog,* vol. 17, pp. 1234-1238, 2004.

[62] *World Health Statistics*. World Health Organisation, 2016.

[63] J. R. Levick, "Overview of cardiovascular system," in *An introduction to Cardiovascular Physiology*, Third ed London: Arnold, 2000, pp. 1-13.

[64] P. Pignoli, E. Tremoli, A. Poli, P. Oreste, and R. Paoletti, "Intimal plus media thickness of the arterial wall: A direct measurement with ultrasound imaging," *Circulation,* vol. 74, pp. 1399-1406, 1986.

[65] T. Gustavsson, Q. Liang, I. Wendelhag, and J. Wikstrand, "A dynamic programming procedure for automated ultrasonic measurement of the carotid artery," *Comput. Cardiol.,* pp. 297-300, 1994.

[66] Q. Liang, I. Wendelhag, J. Wikstrand, and T. Gustavsson, "A multiscale dynamic programming procedure for boundary detection in ultrasonic artery images," *IEEE Trans. Med. Imag.,* vol. 19, pp. 127-142, 2000.

[67] D.-C. Cheng, A. Schmidt-Trucksass, K.-S. Cheng, and H. Burkhardt, "Using snakes to detect the intimal and adventitial layers of the common carotid artery wall in sonographic images," *Comput. Meth. Prog. Bio.,* pp. 27-37, 2002.

[68] T. Nilsson, S. Segstedt, P. Milton, S. Sveinsdottir, T. Jansson, H. W. Persson*, et al.*, "Automatic measurements of diameter, distension and intima-media thickness of the aorta in premature rabbit pups using B-Mode images," *Ultrasound in Medicine and Biology,* vol. 40, pp. 371-377, 2014.

[69] M. Cinthio, T. Jansson, Å. R. Ahlgren, H. W. Persson, and K. Lindström, "New non-invasive method for intima-media thickness and intima-media compression measurements," *Proc. IEEE Ultrason. Symp.,* pp. 389-392, 2005.

[70] J. O. Arndt, J. Klauske, and F. Mersch, "Diameter of intact carotid artery in man and its change with pulse pressure," *Pflügers archiv — Eur. J. Physiol.,* vol. 301, pp. 230-240, 1968.

[71] D. E. Hokansson, Mozersky, D. J., Summer, D. S., Strandness, D. E., "A phase locked echo-tracking system for recording arterial diameter changes *in vivo*," *J. Appl. Phys.,* vol. 32, pp. 728-733, 1972.

[72] A. P. G. Hoeks, C. J. Ruissen, P. Hick, and R. S. Reneman, "Transcutaneous detection of relative changes in artery diameter," *Ultrasound Med. Biol.,* vol. 11, pp. 51-59, 1985.

[73] J. M. Meinders, P. J. Brands, J. M. Willigers, L. Kornet, and A. P. G. Hoeks, "Assessment of the spatial homogeneity of artery dimension parameters with high frame rate 2-D B-mode," *Ultrasound Med. Biol.,* vol. 27, pp. 785-794, 2001.

[74] R. H. Selzer, W. J. Mack, P. L. Lee, H. Kwong-Fu, and H. N. Hodis, "Improved common carotid elasticity and intima-media thickness measurements from computer analysis of sequential ultrasound frames," *Atherosclerosis,* pp. 185-193, 2001.

[75] F. Beux, S. Carmassi, M. V. Salvetti, L. Ghiadoni, Y. Huang, S. Taddei*, et al.*, "Automatic evaluation of arterial diameter variation from vascular echographic images," *Ultrasound Med. Biol.,* vol. 27, pp. 1621-1629, 2001.

[76] M. Cinthio, T. Jansson, Å. R. Ahlgren, K. Lindström, and H. W. Persson, "A method for arterial diameter change measurements using ultrasonic B-mode data," *Ultrasound in Medicine and Biology,* vol. 36, pp. 1504-1513, 2010.

[77] A. Eriksson, E. Greiff, T. Loupas, M. Persson, and P. Pesque, "Arterial pulse wave velocity with tissue Doppler imaging," *Ultrasound Med. Biol.,* vol. 28, pp. 571-580, 2002.

[78] R. Asmar, A. Benetos, J. Topouchian, P. Laurent, B. Pannier, A. M. Brisac*, et al.*, "Assessment of arterial distensibility by automatic pulse wave velocity measurement. Validation and clinical application studies," *Hypertension,* vol. 26, pp. 485-90, 1995.

[79] B. M. Pannier, A. P. Avolio, A. P. G. Hoeks, G. Mancia, and K. Takazawa, "Methods and devices for measuring arterial compliance in humans," *Am. J. Hypertens.,* vol. 15, pp. 743-753, 2002.

[80] E. D. Lehmann, K. D. Hopkins, A. Rawesh, R. C. Joseph, K. Kongola, S. W. Coppack*, et al.*, "Relation Between Number of Cardiovascular Risk Factors/Events and Noninvasive Doppler Ultrasound Assessments of Aortic Compliance," *Hypertension,* vol. 32, pp. 565-569, 1998.

[81] M. Persson, Å. R. Ahlgren, A. Eriksson, T. Jansson, H. W. Persson, and K. Lindström, "Non-invasive measurement of arterial longitudinal movement," *Proc. IEEE Ultrason. Symp.,* vol. 2, pp. 1783-1786, 2002.

[82] T. Nilsson, Å. R. Ahlgren, T. Jansson, H. W. Persson, J. Nilsson, K. Lindström*, et al.*, "A method to measure shear strain with high-spatial-resolution in the arterial wall non-invasively in vivo by tracking zerocrossings of B-Mode intensity gradients," *Proc. IEEE Ultrason. Symp.,* pp. 491-494, 2010.

[83] M. Cinthio, Å. R. Ahlgren, J. Bergkvist, T. Jansson, H. W. Persson, and K. Lindström, "Longitudinal movements and resulting shear strain of the arterial wall," *Am. J. Physiol.-Heart. C.,* vol. 291, pp. H394-H402, 2006.

[84] G. Zahnd, L. J. Maple-Brown, K. O'Dea, P. Moulin, D. S. Celermajer, M. R. Skilton*, et al.*, "Longitudinal displacement of the carotid wall and cardiovascular risk factors: associations with aging, adiposity, blood pressure and periodontal disease independent of cross-sectional distensibility and intima-media thickness," *Ultrasound Med. Biol.,* vol. 38, pp. 1705-1715, 2012.

[85] H. Yli-Ollila, T. Laitinen, M. Weckström, and T. M. Laitinen, "Axial and radial waveforms in Common Carotid Artery: an advanced method for studying arterial elastic properties in ultrasound imaging," *Ultrasound Med. Biol.,* vol. 39, pp. 1168-1177, 2013.

[86] W. W. Nichols and M. F. O'Rourke, *McDonald's Blood Flow in Arteries*, 5th ed. London: Edward Arnold, 2005.

[87] T. Nilsson, S. Ricci, Å. R. Ahlgren , T. Jansson, K. Lindström, P. Tortoli*, et al.*, "Methods for Measurements of the Longitudinal Movement and the Shear-Induced Longitudinal Elastic Modulus of the Arterial Wall," *Proc. IEEE Ultrason. Symp.,* pp. 317-320, 2009.

[88] Å. R. Ahlgren, S. Steen, S. Segstedt, T. Erlöv, K. Lindström, T. Sjöberg*, et al.*, "Profound Increase in Longitudinal Displacements of the Porcine

Carotid Artery Wall Can Take Place Independently of Wall Shear Stress: A Continuation Report," *Ultrasound in Medicine & Biology,* vol. 41, pp. 1342-1353, 5// 2015.

[89] C. Höglund, M. Alam, and C. Thorstand, "Atrioventricular Valve Plane Displacement in Healthy Persons," *Acta. Med. Scand.,* vol. 224, pp. 557-62, 1988.

[90] J. S. Simonson and N. B. Schiller, "Descent of the base of the left ventricle: An echocardiographic index of left ventricular function.," *J. Am. Soc. Echocardiog.,* vol. 2, pp. 25-35, 1989.

[91] V. Bell, S. Sigurdsson, J. J. M. Westenberg, J. D. Gotal, A. A. Torjesen, T. Aspelund*, et al.*, "Relations Between Aortic Stiffness and Left Ventricular Structure and Function in Older Participants in the Age, Gene/Environment Susceptibility-Reykjavik Study," *Circulation: Cardiovascular Imaging,* vol. 8, 2015.

[92] S. Sjöstrand, A. Widerström, Å. R. Ahlgren, and M. Cinthio, "Design and Fabrication of a Conceptual Arterial Ultrasound Phantom Capable of Exhibiting Longitudinal Wall Movement," *IEEE Trans. Ultrason. Ferroelectr. Freq. Control,* vol. 64, pp. 11-18, 2017.

[93] Å. R. Ahlgren, M. Cinthio, H. W. Persson, and K. Lindström, "Different patterns of longitudinal displacement of the common carotid artery wall in health humans are stable over a four-month period," *Ultrasound Med. Biol.,* vol. 38, pp. 916-925, 2012.

[94] H. Liebgott, A. Rodriguez-Molares, F. Cervenansky, J. A. Jensen, and O. Bernard, "Plane-Wave Imaging Challenge in Medical Ultrasound," in *2016 IEEE International Ultrasonics Symposium (IUS)*, 2016, pp. 1-4.

[95] C. Laporte and T. Arbel, "Learning to estimate out-of-plane motion in ultrasound imagery of real tissue," *Med. Image Anal.,* vol. 15, pp. 202-213, 2011.